Miniature and Low-cost Wireless Sensor Platform for Environmental Monitoring (SI-1466)

Final Technical Report
Strategic Environmental Research and Development Program
September 2007

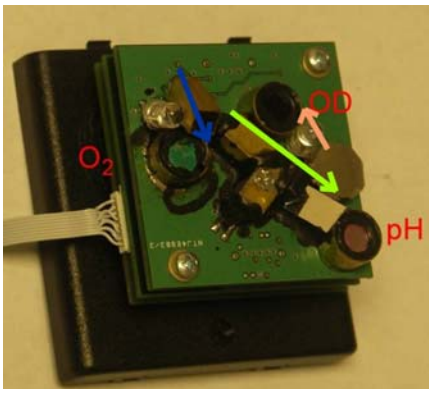

REPORT DOCUMENTATION PAGE

Form Approved
OMB No. 0704-0188

PLEASE DO NOT RETURN YOUR FORM TO THE ABOVE ORGANIZATION.

1. REPORT DATE *(DD-MM-YYYY)*	2. REPORT TYPE	3. DATES COVERED *(From - To)*
15-09-2007	Final	March 2006 - September 2007

4. TITLE AND SUBTITLE

Miniature and low-cost wireless sensor platform for environmental monitoring

5a. CONTRACT NUMBER

5b. GRANT NUMBER

SI-1466

5c. PROGRAM ELEMENT NUMBER

6. AUTHOR(S)

Yordan Kostov
Govind Rao
Upal Ghosh

5d. PROJECT NUMBER

5e. TASK NUMBER

5f. WORK UNIT NUMBER

7. PERFORMING ORGANIZATION NAME(S) AND ADDRESS(ES)

Department of Chemical and Biochemical Engineering
Department of Civil and Environmental Engineering
University of Maryland Baltimore County
5200 Westland blvd, Baltimore MD, 21227

8. PERFORMING ORGANIZATION REPORT NUMBER

DOD 2246

9. SPONSORING/MONITORING AGENCY NAME(S) AND ADDRESS(ES)

Strategic Environmental Research and Development Program

10. SPONSOR/MONITOR'S ACRONYM(S)

SERDP

11. SPONSOR/MONITOR'S REPORT NUMBER(S)

12. DISTRIBUTION/AVAILABILITY STATEMENT

Distribution Statement A: Approved for Public release, Distribution is Unlimited

13. SUPPLEMENTARY NOTES

14. ABSTRACT

A sensor platform with DO, pH, and turbidity sensors was developed. It was equipped with pH and oxygen sensitive fluorescent foils. The foils were attached outside of the waterproof case and read through optical window. They had also antibiofouling protection, which allowed them to operate for extended period of time. A microcontroller switched the channels and collected the reading of O2, pH, and turbidity every 15 minutes, than transmitted it through wires interface to a base station. The platform operates from 4 AA size alkaline batteries. The transmitter has a range of approximately 1 kilometer, depending on the terrain, with transmission rate of 10 kbps

The sensor platform is miniature in size (3"x3"x3" sensing head, electronics and battery pack) and low-cost (~ $450/unit).

15. SUBJECT TERMS

environmental monitoring, wireless sensor platform, optical sensors, dissolved oxygen, pH, turbidity, wireless network

16. SECURITY CLASSIFICATION OF:			17. LIMITATION OF ABSTRACT	18. NUMBER OF PAGES	19a. NAME OF RESPONSIBLE PERSON
a. REPORT	b. ABSTRACT	c. THIS PAGE			19b. TELEPHONE NUMBER *(Include area code)*

Final technical report

Submitted to

Strategic Environmental Research and Development Program

By

Yordan Kostov, Govind Rao
Center for Advanced Sensor Technology and
Department of Chemical and Biochemical Engineering

Upal Ghosh
Department of Civil and Environmental Engineering

University of Maryland, Baltimore County
Baltimore MD, 21250

Contact: Yordan Kostov, tel. 410-455-6569,e-mail: kostov@ umbc.edu

Table of Contents

Figures

Tables

Acronyms and Abbreviations

PAH – Polyaromatic hydrocarbons

TMDL –Total Maximum daily load

DO – dissolved oxygen

pO_2 – oxygen partial pressure

PEG – polyethyleneglycol

LED – Light emitting diode

HPTS – 8- hydroxypyrene-1,3,6-trisulfonic acid trisodium salt

UV – ultraviolet

USB – universal serial bus

A/D – analog-to-digital converter

DR – Decay rate in absence of oxygen

QY – quantum yield

RuDPBP – Ru *tris* (diphenylbipyridine) dichloride

MA-HPDS – hydroxypyrene disulfonic acid methacrylate

PEG-DA – polyethylene glycol diacrylate

OD – optical density

RF – radio frequency

VCCS – voltage controlled current source

TA – transimpedance amplifier

OOK – on-off keying

CRC – Cyclic Redundancy Check

UART - universal asynchronous receiver/transmitter

PC - personal computer

Acknowledgements

The authors would like to thank a number of collaborators from University of Maryland Baltimore County: Dr Appa Anjanappa, Raghavendra Angara, and Jingrui Wang from the Department of Mechanical Engineering, who worked on the mechanical designs and manufacture of the enclosure, Sherif Ibrahim from Department of Chemistry, who worked on the patch synthesis, Albert Hsu from the Department of Computer Science and Electrical Engineering, who worked on the microcontroller firmware, and Sonja Fagervold from the Department of Civil and Environmental Engineering who worked on the calibration tests.

We would like to thank the Strategic Environmental Research and Development Program (SERDP) for the financial assistance which enabled us to undertake this project. Appreciation for technical assistance is extended to Mr. Bradley Smith, Executive Director and Dr. John Hall, Sustainable Infrastructure Program Manager and to the Hydrogeologic, Inc. staff for their administrative assistance.

Executive Summary

The project "*Miniature and low-cost wireless sensor platform for environmental monitoring*" (SI-1466) began on March 15, 2006 and ended on September 15, 2007. The main aim of the SEED project was to provide proof-of-concept of a miniature wireless sensor platform for water quality monitoring. This project successfully developed a small (3"x3"x3") and low-cost sensor node that accommodates three optical sensing devices and transmits the collected data through wireless communication to a base station. The platform was equipped and tested with optical sensors for three common water quality parameters: dissolved oxygen, pH, and turbidity. The platform is amenable to future expansion to include additional sensing elements that are under development at UMBC and elsewhere for the detection of specific contaminants such as CO_2, heavy metals, PAHs, and toxic gases. The project team is actively seeking partners to advance the technology to commercialization.

The key accomplishments in this SEED project are summarized below.

- A low-cost wireless sensor platform was designed and demonstrated for the monitoring of key water quality parameters: turbidity, dissolved oxygen, and pH. The sensor platform was housed in a floating buoy.
- The sensors are based on all-optical technology which excludes direct contact of the electronics with water. They utilize immobilized (and hence non-toxic) fluorescent dyes in the form of peel-and stick patches which are attached to the optics window.
- A miniaturized, rugged 3-channel photometer/fluorometer converts the sensor reading into electrical signal. The signal is digitized by an on-board microcontroller for transmission via a radio frequency link.
- The sensor node collects the data every 15 minutes and transmits it over a wireless link to a base station at distances up to 1800 feet.
- The battery pack (4 AA batteries) can support data acquisition for periods of up to 6 months. The chemical sensors demonstrated currently provide data up to 3 months.
- Sensor patches deployed in streams for up to 4 months did not show signs of biofouling.
- The base station is capable of real-time monitoring of 256 nodes and operates at 433 MHz (the license free ISM band).
- The dimensions of a single node is 3"x3"x3" with a 6" antenna (including the battery pack), and the weight is about 0.5 lb. The sensor node is housed in a floater (buoy) with dimensions 12"x 12"x 6". The cost of one such node (optics, electronics, mechanics) is about $450 in parts and labor.
- With additional funding, the platform is ready for reproduction and deployment as a small network for environmental monitoring. To build on these efforts, a consortium was formed consisting of NOAA, Fluorometrix, Chesapeake Biological Laboratory, and Goddard Earth Sciences and Technology Center, and a proposal was submitted to ONR in response to BAA- 07-040

1. Background

1.1 Introduction

There is a great need for distributed measurements of environmental parameters in DoD sites to meet Total Maximum Daily Load (TMDL) requirements and to gauge sources and dynamics of pollution in large water bodies. Miniaturized and inexpensive sensor platforms, which can be deployed in large numbers over a large monitoring area, are therefore needed. Thus, the development of reliable, miniature, inexpensive, and low power-consuming sensors that can communicate through wireless transmitters to a base station affords a powerful tool in the hands of a site manager to enable necessary environmental stewardship. This project therefore advances the recently developed miniaturized optical sensor technologies into a field deployable platform with remote wireless access capability.

Monitoring of several environmental parameters implies the use of several sensors on a common carrier platform. The platform collects sensor data and transmits them to a central station. Currently, the sensor platforms are relatively big - floats that are several feet long, or moored buoys (Frye et al., 2004). The sensors, designed for use on these platforms, tend to be bulky in design. Development of smaller platforms deployable in water streams requires the use of sensors of a different design.

Currently used commercial sensors are based on a *variety of operational principles*. For example, dissolved oxygen (DO) is usually measured using a membrane covered amperometric cell. The sensor has a current output. pH is measured with a potentiometric electrode with voltage output. Turbidity is measured using an optical transducer by transmission, reflection, or backscattering methods. Conductivity is measured by contact (current through 2 or more electrodes) or contact-less (inductive) methods. CO_2 is rarely measured with sensors. Many contaminants are measured in the laboratory using chromatography. This variety mandates the use of multiple electronic front-ends capable of handling the signal from the transducers. As a result, integration is difficult. A unified signal transducer mechanism would simplify and streamline platform design and operation. *Optical detection* is one of the best candidates for this role. Optical sensors for DO measurements are commercially available[1]. Optical pH sensors are now used in laboratory settings (Liebsch, et al., 2000). Recently, a refractive-index based sensor for measurement of salinity has been reported (Alford, et al., 2005). Turbidity measurement through optical sensing is a mature technique. Other optical sensors (primarily fluorescence based) for various analytes are being developed. The fact that they use the same type of transducer (light emitting diode and photodiode) allows multiple sensors to share the same electronics and makes it possible to miniaturize the sensors.

Previously, some of the sensors have been used for separately monitoring a single environmental parameter – i.e. Yellow Springs Instrumentation manufactures a turbidity probe for use in rivers. Aanderaa makes optical oxygen sensors, which are relatively bulky. Currently, there are no commercial vendors that offer optical pH sensors, and none of the commercially available sensors are integrated with each other on the basis of a common operational principle. The

[1] For example, Ocean Optics (Dunedin, FL), Fluorometrix Inc. (Stow, MA), Presens (Germany), Aanderaa (Norway).

research performed in this project integrates multiple optical sensing elements on a single wireless platform to simultaneously monitor **dissolved oxygen, pH and turbidity**.

1.2 Oxygen measurements

Optical detection of oxygen partial pressure (pO_2) is based on quenching of emission of a fluorescent metal-ligand complex as described previously (Szmacinski and Lakowicz, 1994; Tolosa, et al., 2002). Briefly, the excited state of the luminescent dye (i.e. *tris*(diphenylbipyridine) ruthenium chloride) is collisionally quenched proportionately to the oxygen concentrations, resulting in a change in the emission intensity F and the fluorescence lifetime τ. This process is described by the Stern-Volmer equation,

(1) $$\frac{F_0}{F} = \frac{\tau_0}{\tau} = 1 + K_{SV} \cdot [O_2]$$

where τ_0 and F_0 are the decay time and intensity in the absence of oxygen, respectively, K_{SV} is the Stern-Volmer constant and $[O_2]$ is the oxygen concentration. A typical transfer function of an optical sensor is presented in Figure 1.

The intensity measurements are unreliable due to photodecomposition, instability of the source or detector, scattering or even minor optical changes in the optical path (Kostov, Y., Rao, G. 2003; Mills, 1999). For this reason, lifetime detection is the preferred technique - **fluorescence lifetime** in absence of oxygen is an intrinsic property, and serves as an internal reference. Furthermore, as this is an equilibrium process, neither the analyte, nor the dye is consumed. Consequently, the method has found place in **high-reliability, low power applications (i.e. space shuttle missions**).

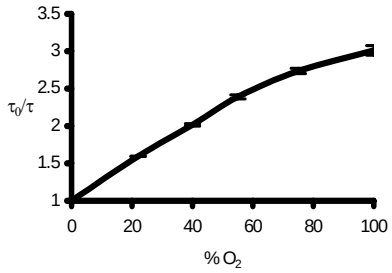

Figure 1. Transfer function of an optical O_2 sensor.

For sensing, the dye is immobilized in a membrane, which prevents the interaction of the dye with aqueous species. This is achieved by entrapping the dye on the surface of 5 μm diameter particles of ion-exchange resin, which is subsequently dispersed in a layer of silicone rubber RTV-117. The resin-bound dye stays in ionized form, which prevents it from recrystallizing. Dye crystals are not oxygen sensitive; resin binding significantly enhances the long-term stability of the sensor. The encapsulation in silicone rubber, which is hydrophobic, prevents the interaction of the dye with the ionic species in water. It does not interfere with the oxygen transfer because of the extremely high solubility of oxygen in the rubber. Another attractive feature is the availability of simple technology for covalent attachment of polyethyleneglycol (PEG) layers (Revzin, et al., 2004), which would serve as protection from biofouling.

In portable instrumentation, a method of choice for the dye's lifetime determination is frequency-domain fluorometry. There, lifetime is measured by illuminating the sensing foil with intensity-modulated light at a frequency ω (ω = 2πf × Hz) generated from a light emitting diode (LED) and measuring the phase shift φ of the resulting emission. The relationship between the lifetime and the phase shift is given by

(2) $$\tan\varphi = \omega \cdot \tau$$

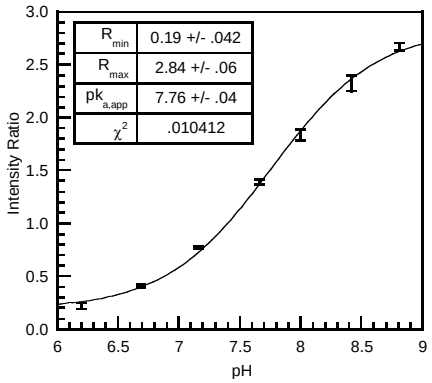

Figure 2. Transfer function of pH sensor.

1.3 pH measurements

Optical pH detection is based on indicator dyes. A successful example is a sensor based on an excitation-ratiometric fluorescent dye (Kermis, et al., 2002; Kermis, et al., 2003). As such, 8-hydroxypyrene-1,3,6-trisulfonic acid trisodium salt (HPTS) is used. HPTS exhibits very high photochemical stability and can be polled at two excitation wavelengths that correspond to the protonated and deprotonated form. It is suitable for ratiometric measurements, which is another method for elimination of the inherent drawbacks of intensity-based measurements. Excitation maxima are at 405 and 455 nm, which allows excitation by ultraviolet (UV) and blue LEDs.

The ratiometric determination using excitation ratiometry of a fluorescent dye is described by the following relationship:

$$R = \frac{I_{\lambda_1} \cdot \phi_{\lambda_1} \cdot \varepsilon_{\lambda_1} \cdot [Ind^-]}{I_{\lambda_2} \cdot \phi_{\lambda_2} \cdot \varepsilon_{\lambda_2} \cdot [H - Ind]}. \quad (3)$$

Here, I_{λ_1} and I_{λ_2} are the light intensities at excitation wavelengths λ_1 and λ_2, ϕ_{λ_1} and ϕ_{λ_2} are the quantum yields of the luminophore at these wavelengths, ε_{λ_1} and ε_{λ_2} are the respective molar absorptivities, [*H-Ind*] is the concentration of undissociated dye, and [Ind^-] is the concetration of the dissociated dye. Recalling that [*H-Ind*]+[Ind^-]=[*T*] ([*T*] is the total amount of the indicator in the sensor (it is known and constant due to immobilization), it is easy to establish the calibration function of the sensor. A typical transfer function of a pH sensor is shown in Figure 2.

The dye is covalently immobilized in a hydrophilic matrix (polyethylene glycol diacrylate). The matrix ensures rapid penetration of the hydrogen ions while successfully preventing the dye from leaching. The PEG membrane also protects from biofouling.

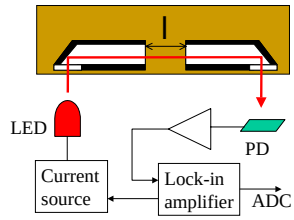

Figure 3. Turbidity setup

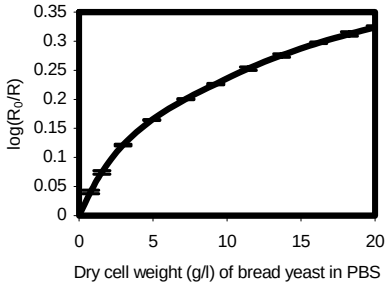

Figure 4. Calibration curve of a turbidity sensor

1.4 Turbidity measurements

Turbidity measurements are performed either using nephelometry (measurements of the scattered at 90º light), the back reflected, or using the standard absorption techniques. In all cases, sample-specific calibration is required. We have developed an absorption-based setup (Kostov, et al., 2002), which has minimal profile and does not disturb the hydrodynamic flow around the sensor (Figure 3). The light is directed at a wedge-like light guide, reflected at 90° and passed through the sample. A second light guide directs the attenuated light toward the photodetector. Lock-in type of electronics is used to measure the light intensity *I*. In addition, the luminance of the LED source I_0 is also monitored. The turbidity *T* then is calculated as:

(4) $$T = \lg \frac{I_0}{I} - k$$

where k is a sample-dependent constant. A typical calibration curve is shown in Figure 4.

The gap length determines the dynamic range of the sensor. Very short gap lengths allow for measurement of very high levels of turbidity, but the resolution of such device is usually insufficient. Determination of the correct path length is usually a result of trial and error. The proposed design allows for selection of various path lengths without substantial change of the device dimensions.

1.5 Integration of the sensors on single platform

The fact that the sensors are based on optical technology is advantageous for a number of reasons. First, it allows positioning of the sensing chemistry outside of the body of a platform and monitoring through an optical window. This allows complete encapsulation of the senor electronics and avoids direct contact with water, which leads to increased reliability and durability.

Another advantage is based on the fact that the amplification and detection hardware can be multiplexed, as the system operates with the same types of signals. The three sensors can share some of the signal conditioning electronics, which results in tighter integration on a single carrier board and low power consumption (?).

The output of a fluorescence based sensor is analog. For data transmission and handling, it has to be converted to a digital form using universal serial bus (USB)-based analog-to-digital (A/D) converter and transmitted to a host computer which performs the necessary calculation to determine the value of the measured parameter. The implementation of an on-board microcontroller with built-in A/D module is trivial. The digitized signal can be transmitted over radio frequency, with a range depending on the available power (and battery). A similar platform, which integrates oxygen and pH sensing (but lacks A/D conversion and wireless capabilities), has been used for monitoring of biotechnological processes.

1.6 Summary of the background

The intention of this SEED project was to expand the application of optical sensors based on the principles described above to environmental monitoring in the field, by integrating them on a single platform, addition of digitization and communications. The common sensing principle allows for shrinking the processing optoelectronics (and eventually some of the filtering optics) into one integrated circuit.

2. Objectives

According to the SERDP 2006 SEED Statement of Need (SON), there is a need to develop miniature sensors for monitoring of water quality parameters. The SON further states:

"Efforts to develop sensors to measure other environmental parameters that relate to general environmental conditions are encouraged. It is desirable that the sensors have long lifetimes in the field, be able to report measurements remotely, as well as produce accurate and repeatable data. The development of small or miniature instruments … is encouraged in order to provide small instrument package profiles for use in the field. The technologies that are developed and tested should be innovative and be able to withstand environmental extremes as well as possible disruption due to military activities"

The objective of this project was to design and manufacture an inexpensive, field-deployable sensor platform equipped with three recently developed miniature optical sensors for dissolved oxygen, turbidity, and pH. The sensor will be able to communicate the collected data, covering a range of 1 mile, to a central server through a wireless network for a period of up to 1 month. The sensors will be based on a common principle (fluorescence) and will share the optoelectronics for detection, ensuring the expandability of the platform toward sensing other pollutants when novel detection chemistries become available.

3. Materials and Methods

The Materials and Methods are included as part of the Accomplishments section below.

4. Accomplishments

The overall project objective to design, prototype, and test a low-cost wireless platform for monitoring of environmental parameters was accomplished. The accomplishments are described below covering the application of sensor chemistry, development of the appropriate optics and electronics, development of the data acquisition software, and testing.

4.1 Chemistry

In this project, chemical indicators that respond with changes in the optical characteristics (spectrum, fluorescence decay rate) as a function of pH or oxygen were used.

4.1.1 Oxygen sensor. Typically, optical oxygen sensing relies on the use of dyes with fluorescence decay rate (DR) in absence of oxygen in the range 100 ns – 10 μs. Ruthenium polypyridyl complexes are used most often because of their high quantum yield (QY) and resistance to photobleaching. Of these, the most widely used is Ru *tris* (diphenylphenathroline) dichloride – a commercially available dye with QY~0.4 and DR~ 5 μs. However, our experience as well as literature data (Hartmann, 2000) suggest that the dye is not quite suitable for long-term (months) measurements. The long-term stability required the use of a dye without the phenanthroline bridge (Hartmann, 2000). The dye that satisfies this requirement was found to be Ru *tris* (diphenylbipyridine) dichloride (RuDPBP), which has QY ~0.2 and DR ~ 1μs. Because this dye is not available commercially, it was synthesized according to a published procedure (Kosch et al., 1998). Briefly, 225 mg RuCl and 800 mg of 4,4'-diphenyl-2,2'-bipyridyl were dissolved in 10 mL acetone, 5 mL of ethylene glycol and 0.2 mL of water and heated under constant stirring until the acetone evaporated. Then, the dark violet solution was refluxed for another 60 min. The color of the solution turned from violet to red-dark brown. After the solution was cooled to room temperature, 50 mL of acetone was added. Ten milliliters of this solution was treated with 50 mL of a 1 M solution of NaCl, upon which a dark-red precipitate was formed. It was filtered, washed with 20 mL of water and 40 mL of ether. The compound was additionally purified using alumina column chromatography.


Figure 5. Oxygen patch

The sensing patch was prepared by first immobilizing the dye electrostatically on silica gel (John et al., 2002) One gram of Davisil, grade 710 (Aldrich) was stirred for 15 min in 20 mL 0.01N NaOH. A solution of 20 mg RuDPBP in 5 mL ethanol was slowly added, and the mixture was stirred for 20 min. The resulting deeply colored particles were filtered out, washed three times with 50 mL deionized water and dried in a vacuum. One gram of silicon RTV sealant 732 (Dow Corning) was dissolved in 5 mL toluene. Two hundred milligrams of the dyed particles were added and the solution was stirred for 6 h. The resulting suspension was spread on a 0.2 mm thick polyester sheet (McMaster) and covered with hydrophobic filtering membrane (Pall). The resulting sandwich was left to dry for 24 hours, and a water-stable, pressure sensitive adhesive (Adhesive research) was attached on the polyester sheet. The resulting patches were cut in squares (0.75"x0.75") and used as peel-and-stick patches for the measurements (Figure 5).

The prepared patches were characterized with respect to the fluorescence decay rate as a function of the oxygen concentration. The patches were measured using frequency-domain lifetime fluorometer ISS Koala (ISS). The results are shown in Figure 6. The lifetime of the fluorescence

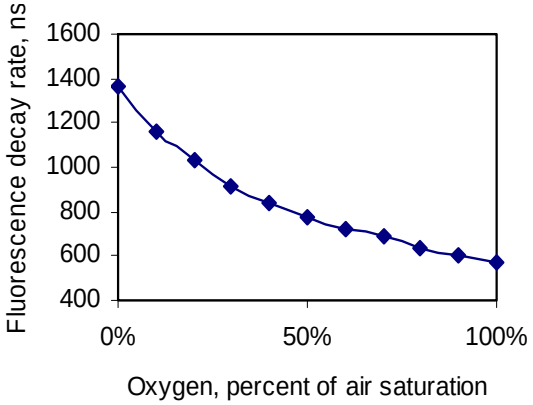

Figure 6. Fluorescence lifetime of immobilized RuDPBP as function of oxygen concentration

steadily decreases from approximately 1.4 μs in nitrogen to around 600 ns in air. This result suggested that the oxygen can be easily determined using frequency domain fluorometry.

However, it was necessary to determine the optimum frequency for the excitation light. For this reason, the phase shift and the modulation plots at different modulation frequencies in air and N_2 were examined (Figure 7). The maximum difference between the phase shifts is achieved when the excitation light is modulated in frequency range 100 - 250 kHz. A closer investigation (results not shown) determined the optimum frequency as 130 KHz. This was the minimum frequency at which the phase shift difference between air and N_2 were greatest (23°C). This phase difference would be the range of the sensor's output when the input changes between 0 and 100% of air saturation. Further increase of the frequency brought only marginal increase of the range (< 1), at the price of significant increase of the modulation frequency, which would result in worse output noise and more complex electronics. When excited with blue light (460 ± 15 nm), the patch emits red light with emission maximum at 630± 15 nm. When the excitation light is modulated at 130 kHz, the resulting signal is ~24° in air and 46° in nitrogen. It was found also that the phase shifts are sensitive to the temperature, ~2%/°C, requiring temperature compensation for field use.

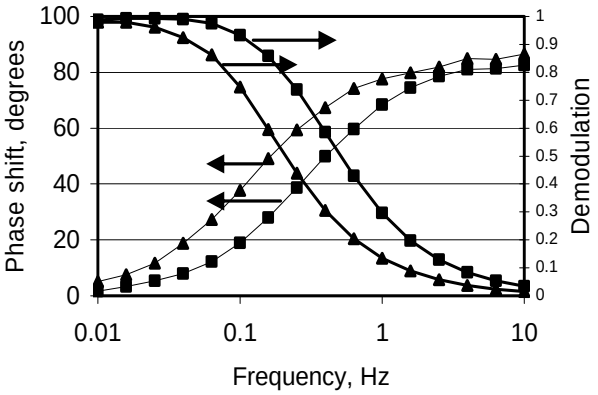

Figure 7. Phase shift and demodulation of the fluorescence of immobilized RuDPBP at different frequencies. ■ – air, ▲- N_2

4.1.2 pH sensor. pH sensor was also synthesized according to published procedure (US pat. No. 7,0209,630). Briefly, the indicator dihydroxydisulphonic acid (100 mg) was dissolved in dimethyl formamide (10 mL) in a 25 mL reaction vessel. Potassium carbonate (1 g) and methacrylic anhydride (1:1 eq., 36 mL) were added. The vessel was closed with a stopper and placed in a 70 °C water bath to react for 12 h. The cooled reaction mixture was filtered. The solvent was removed from the filtrate in a rotary evaporator to yield the crude solid product hydroxypyrene disulfonic acid methacrylate (MA-HPDS).

Figure 8. pH sensitive patch

Next, a silicone layer attached to the top of a polyester foil was prepared to be chemically bonded with the sensing polymeric matrix layer. The activation was performed in two steps: a) oxidation of the silicone and b) creation of an intermediate monolayer between the

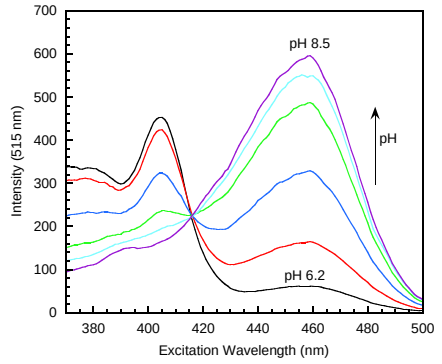

Figure 9. Excitation spectra of the pH sensor

silicone rubber and the future polymeric hydrogel layer. Oxidation was performed in oxygen plasma, at 150 mTorr oxygen pressure, and 100 mW power. Immediately after oxidation the silicone-polyester foil was immersed in DI water for 5 minutes. The foil was then dried in vacuum. The intermediate layer was prepared with methacrylic-reacting trimethoxysilane monolayer. One ml glacial acetic acid was dissolved in 10 ml deionized water, and 200 µl [3-(Methacryloyloxy)propyl] trimethoxysilane (M6514, Aldrich) was dissolved in 20 ml absolute ethanol. 600 µl of the first glacial acetic acid solution was added to the ethanol solution just prior to use. The surface of the oxidized and dried silicon rubber was treated with this mixture for 5 minutes, then washed 3 times with absolute ethanol and dried.

Finally, the derivatized dye MA-HPDS was crosslinked over the silicone. A stock solution of MA-HPDS in deionized water (10 mg/mL) was prepared. Polymer precursor solution was prepared by combining 45 mg of PEG-DA, 200 mL of deionized water,100 mL of the MA-HPDS stock solution and 6 mL of the photoinitiator Darocur and vortexing for 30 min. The solution was spread on the treated silicone and covered with filter paper to provide optical shielding. The solution was polymerized between glass plates to prevent oxygen inhibition and volume contraction of the gel. Free radical polymerization of the acrylate end groups was initiated by exposure to a 100 W long wave UV spot lamp (UVP Inc.; Upland, CA) for 4 min. After polymerization, the foils were washed in deionized water for at least 48 h, with several changes of the wash solution. This step served to both hydrate the matrix and to remove any unbound dye. The resulting patch is shown in Figure 8.

The pH sensor was characterized using steady state fluorometer (Cary Eclipse, Varian).The titration of the sensor with buffers with various pH showed the two excitation peaks of the dye positioned 410 and 460 nm (Figure 10). As the dye fluorescence decay rate is approximately 5 ns, the excitation light can be measured with steady-state excitation. It can be also modulated with practically any frequency below 1 MHz without changes in the amplitude of the fluorescence. Modulation helps to discriminate between the fluorescence and the ambient light, as the sensor has to operate in the field.

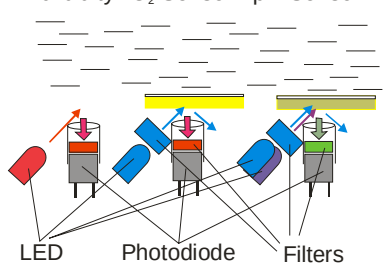

Figure 10. 45° optical path

4.2 Optics

The optics plays a crucial role in the sensor development. The use of two fluorometers and one photometer in a very limited space (3x3") without the use of integrated optics requires the selection of proper filters, orientation of the optical paths to minimize the excitation-emission crosstalk, as well as manufacture of the respective optical devices.

4.2.1 Filters. The selection of the filters was performed with the overall cost of the sensor in mind. As the optical components tend to be expensive, we optimized the cost-performance ratio. In total six optical filters are used in the sensor. As an excitation filter (both for pH and

oxygen), a filter made of Schott glass (BG12) was used. The filter passes wavelengths between 400 and 480 nm and has absorption >4 outside that band. An added benefit of the use of the glass is that the cut-off wavelength does not depend on the incidence angle of the light. Small pieces of the filter glass (5x5 mm) were mounted inside a brass tube and secured with black non-fluorescent glue in place. The light sources were LEDs: violet (emission maximum 400 nm, 8 mW) and blue (emission maximum 460 nm, 6 mW) for the pH sensor, and a single blue LED for the oxygen sensor. Additionally two orange LEDs (emission maximum 605 nm, 3 mW) were used – one as light source in the optical density (OD) detection channel and one as a phase reference for the oxygen sensor (for further explanations, see the electronics section).

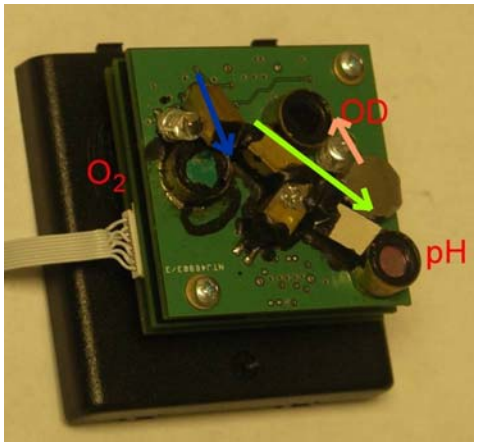

Figure 11. Detection block. The arrows show the spatial direction of light emissions

A long-pass filter with a 600 nm cut-off was used as an emission filter for oxygen. For pH, a band pass filter (550+- 20 nm, Intor) was used. Finally, the receiver of the optical density channel was filtered using red plastic filter with a transmission maximum of 620 nm.

4.2.2 Optical path. An important choice for any optical sensor is the selection of the optical path configuration. In fluorescence measurements, it is typical to select an optical path in which the fluorescence detector is positioned at 90° to the direction of the excitation beam. The reason is the relatively low quantum yield of the emission and the fact that fluorescence is isotropic. As a result, the intensity of the collected light can be several orders of magnitude lower than the excitation light. The wavelength selection devices (filters, monochromators) only attenuate the unwanted wavelengths, but do not completely exclude it. Hence, any additional suppression of the excitation light enhances the signal to noise ratio. From this point of view, the 90° orientation is most favorable because this is the direction of minimum Rayleigh scattering (scattering of the light by the molecules). However, this approach is not possible with fluorophores immobilized in a thin (100 μm) patch. First, it would be difficult to focus the light exactly at the patch edge; second, because of the aspect ratio of the patch (thickness/length = 1/200), the fluorophore would be excited mainly at the edges. For these reasons, it was decided to position the optical axis of the LEDs at 45° in respect to the optical axis of the photodetectors (Figure 10). In this way, the majority of the reflected excitation light travels away from the photodetectors. While the amount of the scattered light is increased, it is still within the range that can be successfully suppressed using filters. Finally, in order to restrict the directionality of the incoming light, an aperture was positioned in front of every photodetector.

It is equally important to position the three optical paths in a way that they do not cross each other. Cross talk may exist if the excitation light from one of the sensors reaches another sensor and the light from it returns in the photodetector for the first sensor. For this reason, a special positioning of the different excitation-emission pairs was adopted (Figure 11). Light paths for oxygen and pH were placed at 45°, and the OD was oriented in the opposite direction, as its emission can readily pass through the detection filters of the other sensors. As this required relatively wide spacing, it was necessary to split the electronics into more than one board in order to fit in the 2x2”footprint.

4.2.3. Beam combiner. Another feature of the developed optics was the beam combiner. As the pH sensitive patch requires excitation at 400 and 450 nm, the LEDs with different emission maxima were used. However, it was found that the prolonged illumination with one of the wavelength (400 nm) results in faster photo bleaching of the indicator dye as compared with the illumination with the other wavelength. As a result, if the two LEDs illuminate two different spots on the sensing patch, after a period of time the patch bleaches at different rates, and the emission intensities from these spots begin to differ, especially over time. This leads to a drift of the sensor signal. To avoid that, a beam combiner that aligns the beams from the LEDs in a single optical path was developed and used. It is based on the use of dichroic mirror with cutoff of 425 nm. Below this wavelength, it transmits the light; however, in the range 425-525 nm, it reflects the light. The LEDs were mounted in a brass holder with a T shape. The dichroic mirror was mounted at 45° to both LEDs (Figure 12). Then, an excitation filter (BG12) was mounted perpendicular to the beam, and finally a mirror was positioned at an angle of 30° to the plane of the LEDs. The mirror ensures the 45° incidence angle with the pH patch discussed above. The back ends of the LEDs were covered with black optical insulator to avoid light leakage. Because the LEDs are non-ideal source (the size of the emitting die is ~10% of the size of the patch), we also considered adding a beam homogenizer after the dichroic mirror. However, this did not change the bleaching behavior significantly, while increasing the size of the device and decreasing the output intensity.

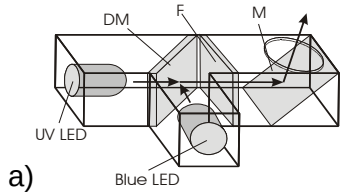

a)

b)

Figure 12. Beam combiner for dual-wavelength excitation. a) schematics, b) picture of the actual device. DM- dichroic mirror, F – filter, M – directing mirror.

4.3 Electronics

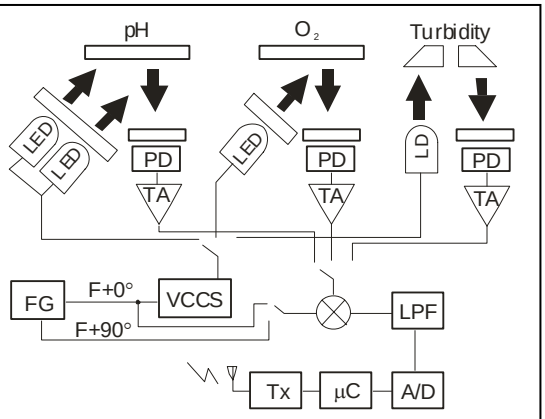

Figure 13 Block schematics of the sensor node. PD – photodiode, FG – Frequency generator, ⊗ - multiplier, µC – microcontroller, Tx – transmitter,

4.3.1 Sensor node electronics.

Sensor node block-schematic is shown on Figure 13. The system consists of 5 functional blocs: light source block, detection block, lock-in detector, control/digitization block and radio-frequency (RF).

Power supply. Currently, the sensor is powered using 4 AA batteries housed in a battery holder. Every block has its own power supply regulator. This allows each respective block to power down if not in use. Furthermore, the voltage requirements in the sensing path are different – the amplifiers and the microcontroller operate at 3.3V, while 4.75V are needed to drive the LEDs. The RF block has its own power supply, which is additionally filtered for better suppression of spurious pulses resulting from the amplification of the RF noise.

Light source block. The excitation light was generated by LEDs. Three types of LEDs were used: blue (emission maximum 460nm), violet (emission maximum 400 nm) and orange

(emission maximum 600 nm). Blue and violet were used in the detection of the pH; orange and blue were used in the detection of oxygen; a single orange LED was used in the OD determinations. The light had to be modulated at a specific frequency in order to reject the ambient light. Furthermore, the light intensity during the peak had to be constant to ensure proper fluorophore excitation. This was achieved by the use of voltage controlled current sources (VCCS) based on common op-amp topology. The LEDs were operated as a floating load. The use of high frequency video amplifiers in VCCS achieved modulation frequencies up to 10 MHz. In our particular implementation, the light was modulated at 10 kHz for the pH and OD sensor and at 130 kHz for the oxygen sensor.

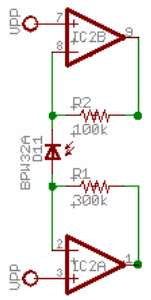

Figure 14. Differential TA

Detection block. At the sensors front end, three photodetectors were used to measure the changes of sensors' optical properties. Photodiodes BPW34S were used. These are large surface (7 mm^2) PIN photodiodes that have minimum capacitance (25 pF at reverse bias 2.5V). As the photodiodes produce current proportional to the intensity of the light, differential transimpedance amplifiers (TA) were used to convert the output into voltage (Figure 14). The use of differential input ensured high common-mode rejection ratio, which was important for detection of current of the order of several pA. The signal was amplified ~100 times in the subsequent stages. In order to avoid simultaneous amplification of the offset voltages, DC, and low frequency noise, the stages were separated using high-pass filters.

Lock-in block. The ability to modulate the light electronically allowed the use of a lock-in detection approach for detection of fluorescence. The lock-in amplifier allows determination of the amplitude *and* the phase of the received signal. Immediately after amplification stages, a synchronous rectifier was used which was driven with the excitation frequency shifted at 0 and 90° of phase. In essence, it operates as a square wave mixer multiplying the incoming signal $A\sin(\omega t+\varphi)$ with the in-phase $\sin(\omega t)$ and quadrature $\sin(\omega t+90)$ of the excitation signal:

(5) $$IP(t)=A\sin(\omega t+\varphi)\cdot\sin(\omega t)=A/2\left(\cos(2\omega t+\varphi)+\cos(\varphi)\right)$$

(6) $$QD(t)=A\sin(\omega t+\varphi)\cdot\sin(\omega t+90)=A\sin(\omega t+\varphi)\cdot\cos(\omega t)=A/2\left(\sin(2\omega t+\varphi)+\sin(\varphi)\right)$$

After rectification, the signal was averaged using a low-pass filter. This operation is equivalent to the removal of the high-frequency components in equations 5 and 6. Hence, after the low- pass filter, only low frequency and DC values are obtained. Their ratio, *QD*/*IP* is equal to the tangent of the phase difference between excitation and the emission fluorescence signal. Similarly, $\sqrt{QD^2+IP^2}$ is equal to the amplitude of the measured signal. In the case of pH, the operational principle requires the detection of two amplitudes (the emission when the sensor is illuminated at two different wavelengths) to find their ratio. The ratio removes the measurement inaccuracies related to the variation of the light path length, positioning of the sensing patch, and attenuation of the light in the illumination path.

In the case of oxygen, the phase shift generated by illumination of the patch with orange and blue light was detected. The orange light was simulating the fluorescence of the patch with zero phase shift. The organge light was used to account for the phase delays introduced by the electronics.

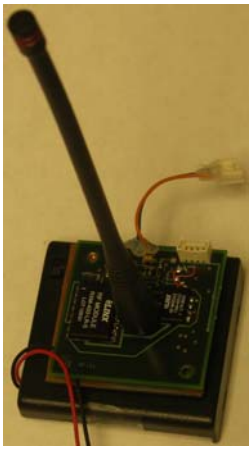

Figure 15. Control and RF block

At the operational frequency – 130 kHz, the phase shift was significant (~43°). It is also well known that the phase shift depends on the ambient temperature. The difference between the phases measured with the use of the blue and the red illumination gave the actual phase shift of the sensor. Measurements of phase shift have the same advantages as the measurements of the spectral ratios.

A picture of the detection block is shown in Figure 11.

Control block. An on-board microcontroller (MSP430F2013) was used to perform the algorithms required for the measurements. In essence this is a system-on-chip with medium complexity and very low cost. The core is built around a very-low-power microcontroller with built-in 16 bit A/D converter and 1.2 V voltage reference. It has on-chip 2kB flash memory and 128 bytes of random access memory (RAM), as well as 16 arithmetic registers. The microcontroller also has 2 digital ports. The digital ports were used to control which part of the node is operational (RF or sensor part). Additionally, the microcontroller addressed the respective measurement channel (OD, pH, or oxygen) and measured the values. It also performed the wireless communication using software based UART. Further details about the microcontroller firmware are given in the software section.

RF block. The communication between the sensor node and the base station was performed using transmitter (TXM430) and receiver (RXM430) modules from Linx technologies. The transmitter and receiver operate at 433 MHz. The frequency was chosen not only because it is license free (ISM band), but also because it penetrates through concrete fairly easily. The modules operate in OOK protocol (on-off keying) where the presence of signal is considered logical 1 and the absence – logical 0. While the protocol has limitation of maximum transmission rate of 10 kbaud, it is advantageous from the point of view of power conservation. For the particular communication, the transmission rate was chosen 2.4 kbaud. As the transmitter and receiver are separate modules, it was decided to use an antenna switch so a single antenna could be used. A quarter-wave whip antenna was used. This ensured circular emission diagram and omnidirectional communication capability. Additionally, this made it possible to mechanically position the antenna in the center of gravity of the sensing node, which made it less prone to being overturned.

Figure 15 presents the external view of the control and the RF block.

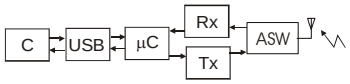

Figure 16 Block-schematics of the base station. ASW- antenna switch, USB – USB controller

4.3.2 Base Station electronics.

The block-schematics of the base station is shown in Figure 16. It is simpler than the node schematics as it performs only communication functions. The base station consists of a microcontroller, which handles the data traffic, a transmitter and receiver module connected to the antenna through an antenna switch, and a USB controller. The microcontroller used is MSP430F1121A, a controller with two independent ports. The base station is powered via the USB. The USB to parallel controller allows transferring a whole byte at a time with ability to control the direction of the transfer through dedicated pins (#RD and WR). The status of the transmit and receive buffers are also indicated at another set of pins

(Ready to receive/Data to transmit). The microcontroller monitors the pins, controls the data direction to the RF modules and respectively switches the antenna switch to enable effective wireless traffic. The first three bits of the Port 1 are multiplexed – when the base station performs data exchange with the USB port, they serve as bits 0, 1 and 2 on the parallel bus; however, in RF mode bit 1 performs the serial communication with the TX and RX modules, while bits 0 and 2 enable and disable the RF modules (see Appendix A). This was done because of the fact that pin 14 itself is multiplexed internally as port bit or as an output of the signal from the microcontroller's timer. The timer is used to generate accurate time intervals for the serial interface.

4.4 Software

The software support consists of three parts:

a) PC software (Labview), which initiates the measurement cycle, receives the data, performs the calculations in order to deduce the value of the parameter from the calibration curve and presents these values in digital and graphical form through user interface;
b) Firmware of the base station (Assembly), which performs the RF transmit-receive protocol functions; and
c) Firmware of the sensor node (Assembly), which performs the RF tasks, scans and measures the sensors.

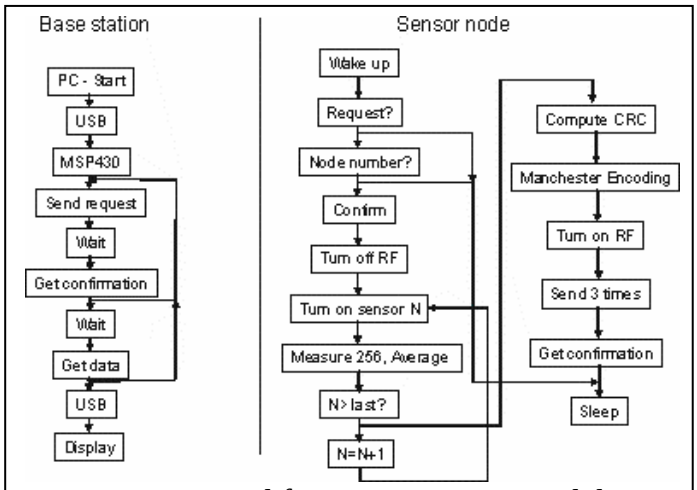

Figure 17. Protocol for communication and data collection

The protocol flow is presented in Figure 17. Every measurement cycle starts with sending the node number that will be polled to the USB serial port. The program uses the freely available DLL drivers from FTDI chip, Ltd. to send two bytes to a virtual COM port. When the FT245R buffer receives the bytes, its RXF# pin goes low. This generates interrupt on port 2 of MSP430F1121A. The firmware of the base station waits for the interrupt in low-power mode, after configuring Port 1 as input buffer, and the respective pin on Port 2 as an input. When the interrupt occurs, the firmware comes out of the low power mode and resumes the main loop. It clocks in the two bytes that form the sensor node address, converts them into a word, calculates the Cyclic Redundancy Check (CRC) and encodes the resulting 4 bytes in Manchester encoding for transmission. In our version of the Manchester encoding, transition 0 to 1 is considered 1 and transition 1 to 0 is considered 0. To every byte, a start and stop bits are added. No parity check is added.

Next, the microcontroller switches the multiplexer to access the RF block, turns on the TX module and configures the pin 14 as an output from Timer A, register 0. The microcontroller then starts the timer and enters a low-power mode. Every time the timer generates an interrupt, it checks the value of the next bit to be transmitted and if needed – toggles the pin. In this way, a software UART transmitter is realized. The data that are transmitted consist of a training

sequence, two wide stop bits (three times wider that the bits in the training sequence) and the data itself (the node number + CRC byte). Three copies of the data are sent to ensure redundancy and better noise immunity. The training sequence is needed due to the fact that the RX modules constantly produce on their output sequence of 0's and 1's due to the input noise. Sending a long sequence of alternating high and low values (i.e. hex55) allows it to be easily distinguished from the noise (the probability of a noise sequence with the same timing as the 128 consecutive bits is very small). The base station sends the data and waits for confirmation that the data has been received. If it does not receive a response within 1 second, it sends the data again, and again waits for confirmation. If after 5 attempts there is no confirmation, the base station sends back to the PC the word hexFFFF, which is decoded as "No answer."

At the receiver side of the sensor node, the receiver watches for the width of the received bit. Normally, there is a constant string of bits (measured as transition high-low-high or vice versa) on the RX module input. The microcontroller monitors that sequence and measures the width of the incoming bit. If the width is within the limits for the expected sequence, the controller counts it as a valid bit and expects the next transition. If the bit is again within the time allotted for it, it is also counted as a valid bit, etc. The microcontroller expects to see a sequence of 122 valid bits in a row. If any of the received bits is not within the specs, the counter of the training sequence is reset and the controller restarts the wait for a valid training sequence.

If all of the 122 bits are received, the microcontroller now expects to see two long bits that indicate the start of the data. These long bits are three time the length of the normal bits. If it sees those bits, the microcontroller advances to the next stage; if not, the receiver subroutine is reset and the process starts over.

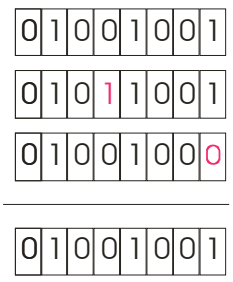

Figure 18. Simple error correction algorithm

If both the training sequence and the start bits are correctly identified, the program advances to the next stage where it functions as a software universal asynchronous receiver/transmitter (UART). It receives the transmitted byte following the detection scheme for Manchester encoding. Then, it splits the data in three (the original data were transmitted 3 times) and begins a procedure that is designed to provide crude error correction: the three sequences are compared bitwise (Figure 18). If all the bits are the same, the bit is correctly received. If one of the three bits is different, the value of the bit is considered to be the value of the other two bits. The approach is based on the fact that during radio transmission, the interferences tend to be of burst type and (usually) alter a sequence of bits in one of the bytes. This is especially true at low data rates employed in the device (2.4 kbaud).

After implementing the algorithm (it can yield wrong results if two bits are erroneous) the program calculates CRC. If the CRC confirms the integrity of the data, the microcontroller proceeds further. If not, it clears the registers and waits the next transmission. The timing of the next transmission is set to accommodate this error correction and checking. The microcontroller finishes the checks before the base station starts the next training sequence and if everything is OK, sends back confirmation. The program attempts the reception up to 5 times; if unsuccessful, it resets.

Once a confirmation has been issued and transmitted back, the sensor node turns off the RF module. This also switches the multiplexer which now connects the first 3 bits of port 1 to the

addressing logic of the light sources and photo detectors. Table 1 describes the codes for the different light sources and detectors. The multiplexing is done for two reasons: a) in this way, the control algorithm is simpler and avoids possible problems with unintentional switching of the RF; and b) better utilization of the microcontroller pins.

Table 1. Codes on the input of the MUX logic and the selected light source, detectors and functions

Code	Sensor	Light source	Photodetector
000	Optical density	OD LED	OD signal photodiode
001	pH	pH blue LED	pH photodetector
010	pH	pH violet LED	pH photodetector
011	Oxygen	Oxygen blue LED In-phase	Oxygen photodetector
100	Oxygen	Oxygen orange LED In-phase	Oxygen photodetector
101	Oxygen	Oxygen blue LED Quadrature	Oxygen photodetector
110	Oxygen	Oxygen orange LED Quadrature	Oxygen photodetector
111	Optical density	OD LED	OD reference photodiode

After issuing the code, the microcontroller measures the output signal from the photodetectors 256 times and averages them. The averaging is done by consecutive addition of every next measurement to a register with carry. After acquisition and summing all the measurements, the result is simply shifted right one byte. The sensors are scanned consecutively to acquire the measurements from all of them. Then, the data are converted (according to the already described algorithm) in serial format, Manchester encoding, the sensor node number is added and CRC is calculated. The 18 bytes are transmitted back to the base station, which does error correction, CRC check and transmits via USB the results.

The personal computer (PC) program for the control, which initiates the measurement, serves as a tool for selection of the sensor node and as a visual interface for data display. As it receives the raw measurements from the sensors, it calculates the quantities that are related to the measured values:

Optical density:

(7) $$OD = \lg \frac{I_{ref}}{I_{sig}}$$

pH:

(8) $$pH = \frac{I_{blue}}{I_{violet}}$$

Oxygen:

(9) $$DO_{phase} = \arctan \frac{I_{blue}^{In-phase}}{I_{blue}^{Quadrature}} - \arctan \frac{I_{orange}^{In-phase}}{I_{orange}^{Quadrature}}$$

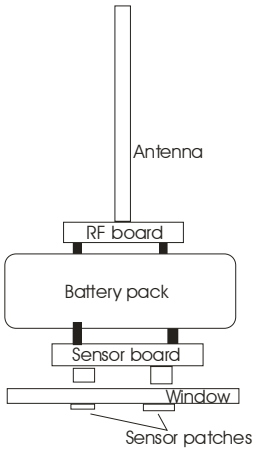

Figure 19. Mechanical positioning of the sensor components

Using the calculated values and the generated calibrations, the software displays the respective measurements of optical density, dissolved oxygen and pH.

4.5 Mechanics

The mechanics of the sensor ensures: a) the positioning of the optoelectronics in their respective environments; b) protection of the electronics from shocks, water and moisture; and c) the floatability of the device.

4.5.1 Positioning the electronics. The sensing patches and the observation window have to be submerged in the water. However, in order to ensure relatively long transmission range, the antenna has to be outside of the water (Figure 19). As the goal was to make a compact block, it was decided that the electronics boards will be attached to the battery pack so the top side carries the RF modules, microcontroller and the antenna, and the bottom part carries the sensing optoelectronics. As the battery pack is the heaviest construction element, it serves as a carrier for all the other elements attached using posts.

4.5.2 Protection from water.

The primary function of the enclosure is to keep the sensor afloat while keeping the sensing window submerged in water. The size was designed to have the gravity and the water displacement forces balanced when the floater is submerged to approximately one half of its height. To enhance stability in water, the cross-section of the enclosure was selected to be trapezoidal. Tilting to one side produces rapidly growing displacement of water which pushes the floater back to the upright position. The dimensions of the floater are selected to be approximately 5 times wider than the battery pack, which ensures the stability of the floater and decreases the probability for turn-over. In the case of turn-over, the floater center of gravity is out of the water, and even a small disturbance will flip it back into upright position.


Figure 20. Side view of the floater

The encasement is designed to have two cavities: internal, which holds the electronics in place and protects it from shocks (0.5” plastic) and external, which is filled with Styrofoam to ensure the floatation (Figure 20). The Styrofoam was added as a backup floatation medium in case the there is a crack in the external cavity of the floater.

The internal cavity features a circular opening through which the antenna projects out. It is also insulated from the environment with a plastic tube. The final designs are shown in Appendix B.

4.5.3 Sensor window. One of the most important parts of the enclosure is the optical window. It was made out of UVA-transparent plastic in order to allow for the 395 nm excitation for the pH sensitive patch to come through. This excluded the use of polycarbonate, which otherwise would be excellent choice because of its superior mechanical characteristics. In this version, the optical window was manufactured out of a 0.25” acrylic polymer. However, future versions of the floater should utilize either glass or cyclic polyolefin as window material because

Figure 21. Floater sensor window (left) and the sensor patches mounting (right)

of their excellent environmental stability, high transparency to the UV and minimum penetration of water vapor.

The window is secured in place by a metal holder (Figure 21) with a rubber gasket. The water proofing of the gasket is provided by application of silicon grease. The circular shape of the window allows easy positioning without misalignment. Patches are attached to the front window either using pressure-sensitive adhesive, or silicone grease.

4.6 Tests

4.6.1 Range. The range of the Lynx modules according to the datasheet is up to 3000 feet. Our tests with the evaluation modules showed similar distances (2800 feet with no obstacles. 2200 feet with some obstacles). The evaluation modules consisted of a single transmitter and receiver on two separate boards. The boards were equipped with antenna for each transmitter and receiver. However, the design of the floater required the use of single antenna. Hence, the transmitter and the receiver both on the sensor node and the base station were multiplexed through an antenna switch. The actual range of reliable transmission in this case was 1800 feet with no obstacles and 1200 feet with obstacles.

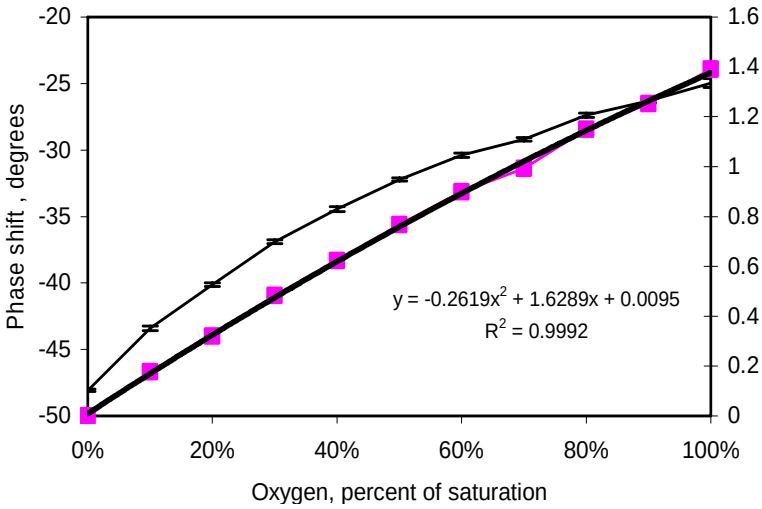

Figure 22. Oxygen sensor calibration

4.6.2 Oxygen calibration. The sensors were extensively calibrated in the lab. Oxygen calibration is presented in Figure 22 (upper curve). The sensor was challenged with a gas mixture which consisted of air and nitrogen by blending the respective gases at predefined flow rates. The flows were measures using precision rotameters. The output phase was calculated using equation 9. The measurements of the phase were performed on average 50 to 70 times at every gas concentration. The resulting error bars are also presented in Figure 22. As can be seen, the relationship was found to be non-linear. The phase readings were highly repeatable – the phase noise of the reading was on average 0.16 degrees, or 0.5% of the reading. The highest uncertainty of the reading was at oxygen saturation (0.33 degrees, or 1.3% of the reading), and the lowest – in absence of oxygen, 0.1 degree, or 0.2% of the reading. Based on the noise results it can be concluded that using the combination of the selected dye and the electronics, the sensor can easily perform measurements with accuracy of ~1% at high oxygen concentrations and better than 0.5% at low oxygen concentration. It is also worth noting that the sensitivity of the sensor increases with the decrease of oxygen concentration.

The data were fitted to the Stern-Volmer equation which takes the following form when describing the dynamic quenching of a fluorophore by a quencher:

(10) $$\frac{\tau_0}{\tau} = 1 + k_{SV}[O_2]$$

Here, τ_0 is the fluorescence decay rate of the dye in absence of the quencher (oxygen), τ is the decay rate at current oxygen concentration, k_{SV} is the Stern-Volmer coefficient, and $[O_2]$ is the oxygen concentration. The tangent of the phase shift tan φ is proportional to the lifetime τ of the dye:

(11) $$\tan\varphi = 2\pi f \cdot \tau$$

where *f* is the excitation light modulation frequency. Substituting equation 7 in equation 6 yields

(12) $$\frac{\tan\varphi_{N_2}}{\tan\varphi} = 1 + k_{SV}[O_2]$$

Based on equation 12, we calculated $\frac{\tan\varphi_{N_2}}{\tan\varphi} - 1$ at different oxygen concentrations. The results are plotted also in Figure 22 (squares). Attempts to find a good linear fit were unsuccessful; although the regression coefficient was as high as 0.9962, the difference between the actual oxygen concentration and that calculated from the fit was in some instances as much as 0.035 (absolute difference), and the model was predicting negative oxygen concentration when the actual value was zero. The second order polynomial fit gave significantly better results: correlation coefficient R^2=0.9993, and the differences in all cases were less then 0.009 (absolute difference), on average 0.0055 (excluding the obvious outlier of the measurement at 70% of air saturation, which was most likely caused by an error in gas flow settings during the calibration).

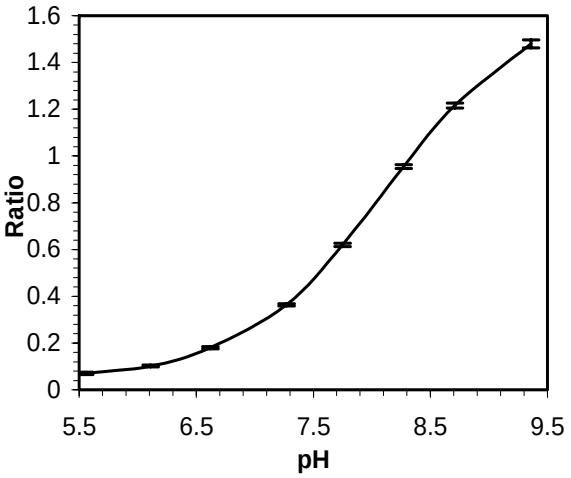

Figure 23. pH sensor calibration

Finding a non-linear Stern-Volmer plot is not unusual; it often occurs when the dye is immobilized on the solid support. However, the important result was that it is possible to generate a simple transfer function that yields highly accurate prediction of the oxygen concentration.

4.6.3 pH calibration. pH calibration was performed by exposing the sensor to different pH buffers, ionic strength ~ 10 mM. The sensor response was calculated according to equation 8. The results are presented in Figure 23. Again, the readings were averaged out of 50 to 70 readings at the same concentration. The error bars are also presented in the same figure. As can be seen, the accuracy of the measurement is relatively high – the error of the reading is approximately 6.3% at the lowest pH of the range and drops below 1% at the highest pH. In terms of pH error, this results in accuracy of pH better than 0.03 pH units. An attempt was made

to fit the curve to the known relationship between pH, the apparent dissociation constant of the dye pK_a, and the measured ratio R:

$$pH = pK_a + \lg\frac{(R_{\min} - R)}{(R - R_{\max})} \quad (13)$$

Here R_{min} and R_{max} are the measured ratios at the end of the pH range (i.e. 3 pH units away from the pK_a). However, the fit was unsatisfactory – the calculated pH differed from the actual values as much as 0.25 pH units, which was clearly unacceptable – the commonly used accuracy of the glass pH electrodes is ~0.05 pH. Hence, it was decided not to use equation 9 for calculation of pH (although it would have significantly simplified the calculations). Instead, a procedure based on the piecewise approximation of the calibration curve was adopted. The curve was considered to be a straight line in between the measurement points and the pH was calculated from the linear fit.

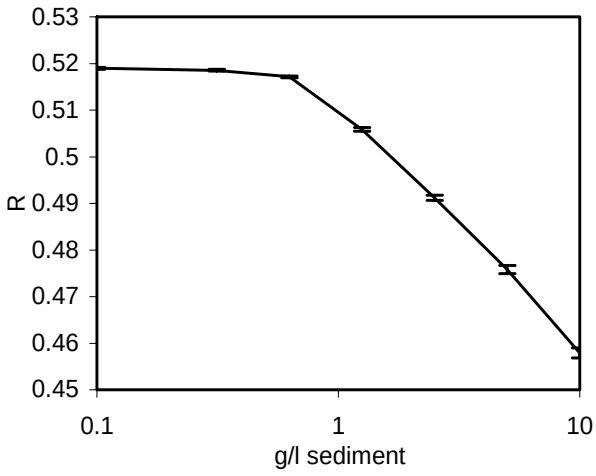

Figure 24. Calibration of the turbidity sensor

4.6.4 Turbidity sensor. The sensor uses the simplest possible configuration for measuring turbidity. This is a single beam photometer that operates by detecting back reflected light. It was calibrated by diluting different amounts of river sediment and presenting them in front of the sensor optics. The sensors output was calculated using equation 7. The results are presented in Figure 25. Once again, the presented data points are an average of 50 to 70 readings at the same concentration. The error bars are also presented. The standard deviation of the measurements was also quite low – from 0.2% of the reading at low sediment concentration to ~1% at the highest sediment concentration. The decision was made not to use formazine as a calibration standard as it is usually quite different from the actual value of the suspended solids. As with any turbidimeter, the actual reading will be strongly dependent not only on the turbidity, but also on the absorption of the water at the emission wavelength of the used light source. It was decided that instead of a theoretical description of the transfer function (such as the formula for the Rayleigh scattering) a piecewise approximation of the calibration will be used.

4.6.5 Temperature coefficient and ionic strength errors. As the sensors are intended to work in the field, they will have to work in a wide range of temperatures (i.e. 0-50 °C). For this reason, the sensors were evaluated for their temperature stability. It was found that the turbidity and the pH sensor do not exhibit measurable temperature sensitivity. The turbidity sensor is referenced by measurement of the light source intensity, and any variations due to temperature are canceled out. The pH sensor works by measuring the ratio of the emission intensity; if the temperature increases, the absolute fluorescence intensity will decrease, but the ratio will remain stable. As long as the ratio for the excitation light intensities remains the same, the sensor will be temperature insensitive. Indeed, that was the case with the selected GaN LEDs. If LEDs with the

same temperature coefficient are not available, an intensity monitoring network would be desirable.

The oxygen sensor, on the other hand, showed sensitivity toward temperature changes. It was approximately 2.5%/°C. The calibration curve was clearly reproducible at different temperatures with no hysteresis. This implies that the oxygen concentration could be easily deduced using temperature correction.

4.6.6 Long-term stability of the sensors. As the sensors are intended for use over extended periods of time, it is important that the sensors give a stable reading. The longevity of the sensor platform in the field is determined by 2 factors: a) the capability of the battery to support the RF transfer and the measurements, and b) b the long-term stability of the chemical sensor (oxygen and pH). The turbidity sensor does not involve any chemical sensors, so its operational life is determined solely by the electronics.

A) Power budget: The power use during 1 measurement cycle is 0.033 mAh (one cycle last approximately 2 seconds). The power use during 1 transmit/receive cycle is 0.0006 mAh. The sensor node is powered from 4 AA batteries, with capacitance of approximately 1700 mAh. The stored power should suffice for ~ 50000 measurements. At a rate of 5 measurements/h, the battery should last a little over a year. During the tests, the receiver was constantly on (this made it easier for establishing the communication with the sensor node and somewhat simplified the firmware programming). Under this condition, we have observed the battery to last ~ 2 months. One concern, however is the possibility for the internal resistance of the battery to rise to the point where the current, delivered for the measurements, will be limited below the level set by the current source. In this case, it would start affecting the intensity of the LEDs. While it is not of a concern with regard to the oxygen and turbidity sensors, it might affect the pH measurements. The reason for that is their different volt-ampere characteristics. We are in the process of verifying this possibility.

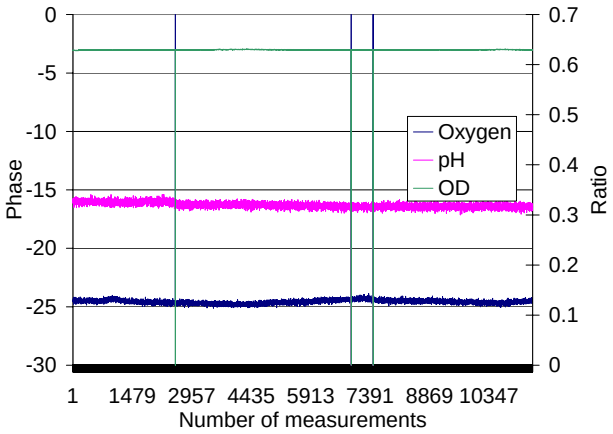

Figure 25 Stability of the sensors

B) Sensor long term stability: The long term stability of the sensors is affected mainly by the dye bleaching. In order to extract the information, the dye is illuminated with highly energetic (violet and blue) light with relatively high intensity (~0.7 mW). This resulted in gradual photodeterioration of the dye. When in an excited state, all dyes are prone to photochemical reaction (i.e. photo oxidation), which is facilitated by the light energy. As the sensors are used, they gradually bleach. To a significant extent, the influence of the bleaching is offset by the ratiometric measurements (in the case of pH) and the phase measurements (in the case of oxygen). It allows continuing the measurements, with the most significant consequence of gradual increase of the noise of the measurement when the sensing patches are bleached. We attempted to recreate this scenario by accelerated aging. As the bleaching is a function of the dose of light that the sensor receives, we tested the sensors at the fastest possible reading rate (i.e. once every 2 seconds). The results are shown in Figure 25. We performed ~ 11000

measurements in a row. At a rate of 5 measurements per hour (which is a high speed for environmental monitoring), this is equivalent to 3 months of continuous measurements. As expected, there is no measurable drift on the turbidity sensor. The drift of the pH sensor was equivalent to approximately 0.02 pH units, which an excellent stability even for a standard pH electrode. The overall drift of the oxygen sensor was approximately 3% of the oxygen reading (absolute value). However, on the plot there are easily discernable day and night cycles. Our conclusion was that this is a consequence of the oxygen sensor's temperature coefficient. With addition of a temperature measurement, the reading can be successfully corrected and even smaller drift achieved.

Figure 26. Research assistant Sherif Ibrahim sets an experiment on biofouling of the sensing membranes in the nearby stream.

4.6.7 Biofouling tests. An important feature of the chemical sensors is the resistance to biofouling. The pH sensors have natural protein repellent capabilities, as their surface is covered with poly (ethyleneglycol) hydrogel. It repels proteins and is often used also as cell repellent material. More of a concern was the oxygen sensor, as its surface is hydrophobic. In order to prevent cell attachment, we used Teflon tape as optical shield. It has low surface energy and even a minute flow (such as the one in a stream) will easily remove any sticky cells on its surface. We set a test on biofouling in the nearby slow-running stream. The membranes were attached to a floater and anchored in the middle of the water flow. Every week the membranes were taken out and evaluated under a microscope for biofouling. We attempted to stain any attached cells or proteins with Methylene Blue. Teflon and silicone rubber (sensor materials) are not stainable with this stain. In a four week period, no attached cells were found. Further testing was stopped due to the deteriorating weather and the loss of the floater due to a flooding in the stream caused by the remnants of the hurricane Ernesto.

4.7 Sensor node dimensions and weight

The dimensions of the sensor electronics are 2x2". It is mounted on the battery compartment which measures 2.5x2.5x0.5". Without the antenna (but with the mounting brackets) the system fits in a volume of 3x3x3". The antenna length is 5". The floater is 10x10x4", with an additional tube for antenna protection. The sensor node electronics weighs about 0.5 lb. With the enclosure, the weight is approximately 2.5 lb. If the enclosure is manufactured out of metal, the weight will increase accordingly.

4.8 Cost

The cost of the materials and labor for manufacturing (small series, < 10 pcs.) is approximately $450/unit. Materials include electronic components and batteries, printed circuit board, optics and mechanical parts. After the boards have the parts soldered in, it would take a skilled

technician 3 to 6 hours to assemble the optics and electromagnetic shields, glue together the carrier posts on the battery holder, and program the microcontroller. The labor time to assemble the mechanical enclosure is also about 6 hours.

5. Conclusions

This SEED proposal was aimed at providing the proof-of-principle that a wireless integration platform can be built for available and emerging optical sensors that can detect a wide range of environmental parameters. The project demonstrated a wireless low-cost sensing platform for environmental monitoring which can be used to continuously measure oxygen, pH and turbidity for an extended period of time without servicing. If a number of platforms are deployed, they can be used as a wireless sensor network for monitoring of water quality in a large water body.

5.1 Transition Potential

The project was focused on transitioning the latest advances in optical sensing developed in the field of biomedical sciences to environmental applications. The Center for Advanced Sensor Technology at the University of Maryland Baltimore County has a long history of transitioning technologies developed in academic settings into commercial products. One example is our relationship with Fluorometrix, Inc. (Stow, MA), www.fluorometrix.com that licensed our technology and successfully put on the market a line of optical sensors for use in shake-flask experiments. The proposed sensor platform can easily become an extension of their existing production line, as the company already has licensed the core technology. When we enter the next stage of network development (i.e. manufacturing of a set of platform nodes and their deployment), Fluorometrix, Inc. will be our partner. However, this is a small start-up company that still struggles for its survival, so it is unlikely that they will be able to share the cost. We also intend to look for other industrial partners.

Our new approach of integrating multiple optical sensors on a common wireless platform can find numerous uses in the Department of Defense and private industry. Such a platform has great potential for adoption not only for environmental monitoring of pollutants, but will also have applications in advanced sensing and warning systems against biological or chemical attack or accidental release of chemicals in an industry.

To help in the transition of the technology, the research team presented the information at the 234 National Meeting of the American Chemical Society in the section “Environmental sensors and networks”, as well as at the SERDP symposium. Currently, we are in talks with Claire Welty, Director of the Center for Urban Environmental Research and Education at UMBC and Cherie V Miller from USGS to allow us to use one of their test sites to deploy the platform continuously. We are also preparing a manuscript for submission to the journal “Environmental Science and Technology”. In collaboration with Chesapeake Biological Laboratory and Goddard Earth Sciences and Technology Center, we also hope to use the technology in the Chesapeake Bay through a project proposal submitted to the Office of Naval Research.

5.2 Future work

During the work on the current prototype, we determined several technological issues as well research needs that need to be addressed in the next stages of the project. The technological issues are:

a) Temperature measurements. In order to eliminate the small temperature drift of the oxygen sensor, temperature needs to be measured and transmitted. This can be easily achieved, as the microcontroller in the sensor node is equipped with on-chip temperature

sensor. A small programming change in the firmware (both in the sensor node and the base station) would resolve the issue. If, however, the tests prove that there is a significant temperature gradient between the sensing patch and the electronics, the temperature sensor can be incorporated in the sensing patch (i.e. temperature sensitive dye).

b) 4-beam turbidimeter. Currently, the platform features a single beam turbidimeter. While this is a reliable device, its range and linearity may be not sufficient. The best in class are the 4-beam turbidimeters, which can be easily implemented on the platform.

c) Communication range improvement. While the current range can be sufficient for many small–area networks, longer ranges are desirable. The manufacturer of the RF modules has just started offering a new RF module which combines the transmitter and the receiver into a single module, which requires only a single antenna. The elimination of the antenna switch in our design will immediately increase the range back to~ 2800 feet with little change in the power budget. We have also started investigating the use of another transceiver, CC1000 (Texas Instruments), which is capable of achieving a range of up to 3 miles with just 20% increase of the power budget. Finally, the software can be adapted to allow the data to be communicated between the sensors, so every sensor in series can act as a relay station.

d) Energy harvesting from the environment. Although the energy conservation is important, supplementing it using, for example, a solar cell, can significantly extend the non-service life of the platform. However, this would require the use of rechargeable batteries and addition of a charging circuit on the boards.

e) Better mechanical enclosure. Current enclosure (floater) was manufactured out of plastic in order to speed up the prototype development and to simplify the assembly. However, for extended service a more durable enclosures will be needed (i.e. sheet metal). As it is somewhat heavier, the designs will be slightly different. On the other hand, it will provide better protection from the elements.

Additionally, more research may be needed on the following topics:

a) Better energy conserving algorithms. Better energy utilization can be achieved by using the LEDs for shorter time and turning off the receiver when not used. Currently, the LEDs have to be on for at least 250 ms to ensure accurate reading. Decreasing the time constants will reduce the needed on-time, but will also worsen the signal-to-noise ratio. Further research is needed to determine whether significant decrease of the reading will produce measurements with acceptable accuracy.

b) Modification of the pH dye to exhibit less ionic strength stability. Earlier measurements of the sensing dye showed that it exhibits some drift due to the ionic strength of the sample. Usually, the river waters have fairly low ionic strength; however, during intense flooding it can significantly increase. Hence it is desirable to minimize the signal drift due to the dye properties. As follows from the Debye-Hueckel theory, a method to achieve that is to decrease the number of the dissociating groups on the dye. Currently, it has three such groups – one hydroxyl group, which ensures the pH sensing capabilities, and two sulphonic acid groups, which impart water solubility, but are non-essential for

the pH sensing. Their derivatization to non-dissociating groups would decrease the sensitivity to ionic strength 3 fold.

c) Implementation of antibiofouling surface treatment for all sensing surfaces. The antibiofouling tests did not show any growth on the patches. Part of the reason for this is probably the fact that they were anchored in the middle of a stream with relatively high water flow. However, this is not always possible or desirable (due to the possibility for the platform to be washed away). Hence, additional surface treatment may be desirable for the patches. One option is to treat all surfaces with PEG hydrogel. Another possibility is to use some substances that are regularly used in the biomedical field (i.e. phosphatidyl choline).

d) Deployment of a sensor network. In order to actually make a network, several nodes need to be deployed. This will address the need to resolve any possible issues with the RF traffic and to compare possible sensor-to-sensor variations. It will also allow evaluation of the work of the system as a whole.

e) Long-term field use of the network. Lastly, a relatively long-term (~ 1 year) study is required to verify the performance of the system in real world conditions.

6. Literature Cited

1. Alford, M.H., Gerdt, D.W Adkins, C.M., (2005) An Ocean Refractometer: Resolving millimeter-scale turbulent density fluctuations via the refractive index. *J. Atmos. Ocean. Technology* (in press). Available at http://opd.apl.washington.edu/scistaff/bios/alford/assets/alfordetal05b_pp_LR.pdf
2. Frye, D., Hogg, N., Wunsch, C. (2004) A Long Duration Mooring For Ocean Observation. *Sea Technology* **45**, issue 6, 26.
3. Hartmann, P. (2000) Photochemically Induced Energy-Transfer Effects on the Decay Times of Ruthenium Complexes in Polymers. *Anal. Chem.* **72**, 2828-2834
4. John, G.T., Klimant,I., Wittmann, C., Heinzle, E. (2002) Integrated Optical Sensing of Dissolved Oxygen in Microtiter Plates: A Novel Tool for Microbial Cultivation. *Biotechnol.Bioeng*, **81**, 829-836
5. Kermis, H.R., Kostov, Y., Harms, P., Rao, G. (2002) A dual-excitation ratiometric fluorescent sensor for non-invasive bioprocess monitoring: development and application. *Bitechnol. Prog.* **18**, 1047-1053
6. Kermis, H.R., Kostov, Y., Rao, G. (2003) Rapid method for the preparation of a robust optical pH sensor. *Analyst* **128**, 1181-1186.
7. Kosch, U., Klimant, I., Werner, T., Wolfbeis, O.S.(1998) Strategies To Design pH Optodes with Luminescence Decay Times in the Microsecond Time Regime *Anal. Chem.* **70**, 3892-3897
8. Kostov, Y., Harms, P., Rao G. (2002) On-line optical density measurements in shake flasks. *224th ACS National Meeting, Boston MA, August 2002.*
9. Kostov, Y., Rao, G. (2003) Ratio measurements in oxygen determinations: wavelength ratiometry, lifetime discrimination and polarization detection. *Sens. Actuators B* **90**, 139-142.
10. G. Liebsch, G., I. Klimant, B. Frank, G. Holst, and O. S. Wolfbeis. (2000) Luminescence Lifetime Imaging of Oxygen, pH, and Carbon Dioxide Distribution Using Optical Sensors, *Appl. Spectrosc*. **54**, 548-59.
11. Mills, A. (1999) Response characteristics of optical sensors for oxygen: models based on a distribution in t_0 or k_q. *Analyst* **124**, 1301-1307.
12. Revzin A., Rajagopalan P., Tilles A.W., Berthiaume F., Yarmush M.L., Toner M. (2004) Designing a Hepatocellular Microenvironment with Protein Microarraying and Poly(ethylene glycol) Photolithography, *Langmuir* **20**, 2999-3005
13. Szmacinski, H., J. R. Lakowicz,. (1994) in *Topics In Fluorescence Spectroscopy* (ed. Lakowicz, J. R.) 295 (Plenum Press, New York, 1994).
14. Tolosa, L., Kostov, Y., Harms, P., Rao, G. (2002) Noninvasive measurement of dissolved oxygen in shake flasks. Biotechnology and Bioengineering 80, 594-597.

Appendix A

Base Station Electronics

Appendix B

Mechanical design of the system

Appendix C

Papers and Presentations

Appendix A

Base Station Electronics

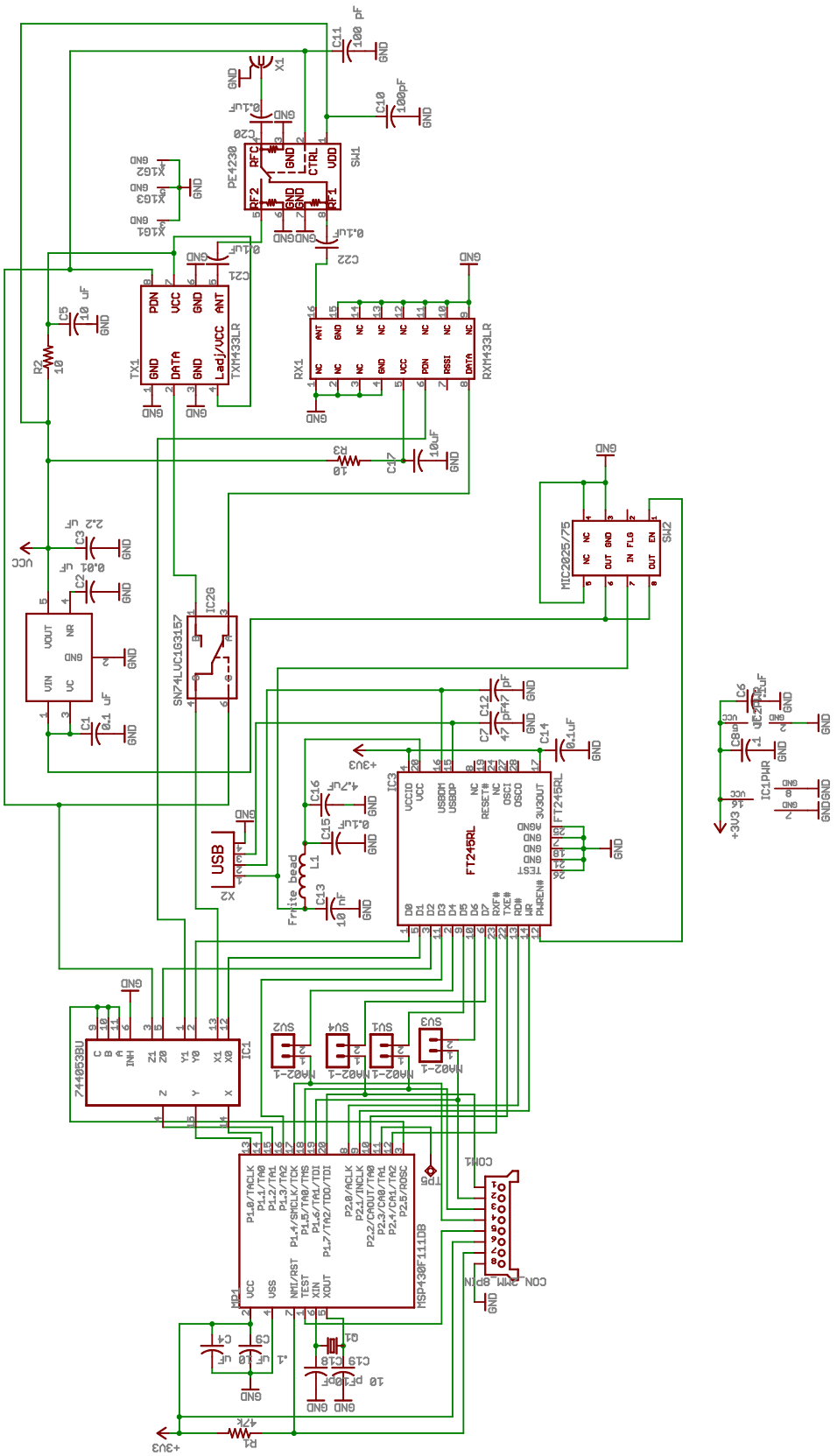

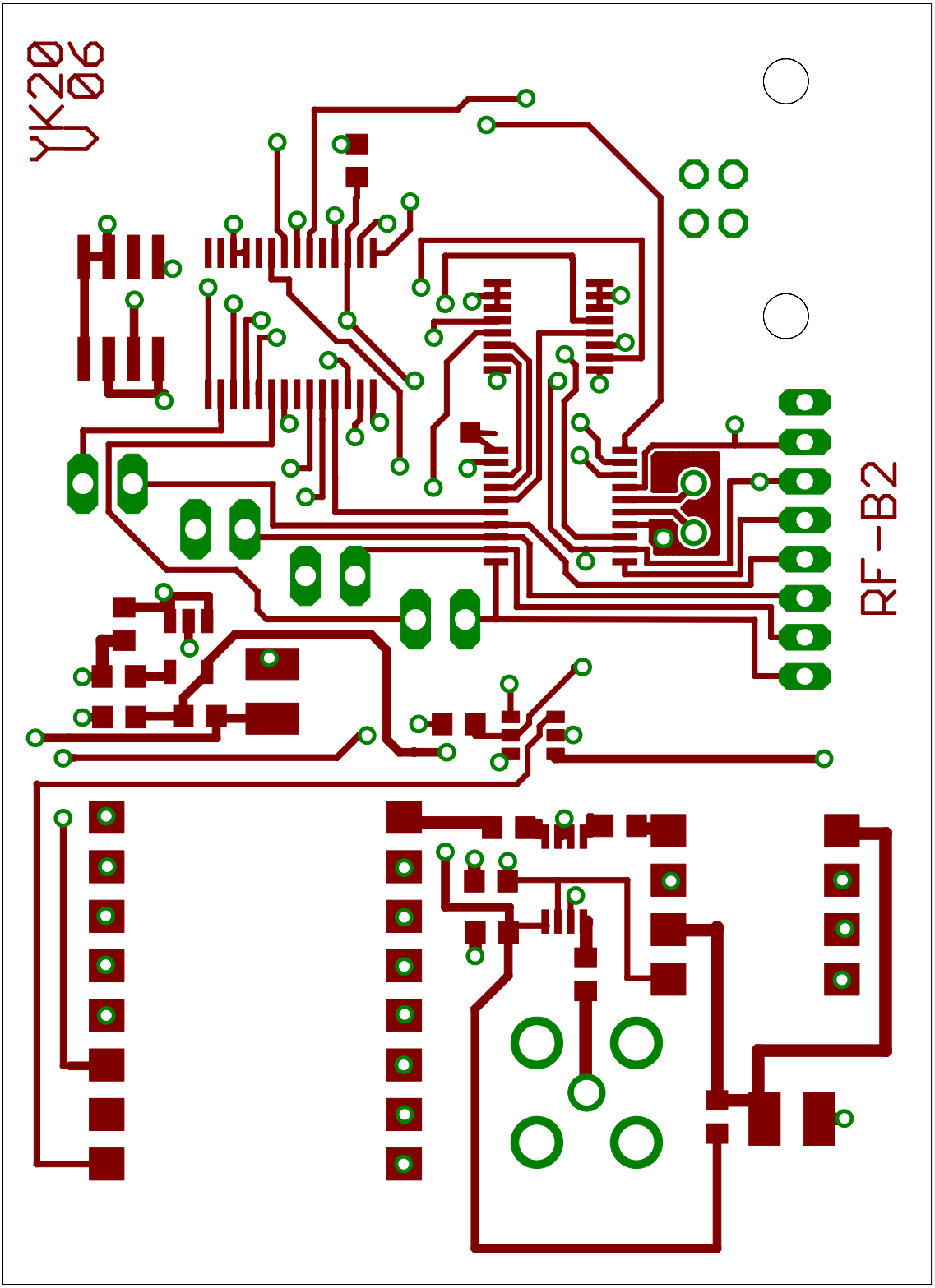
YK20
YK06
RF-B2

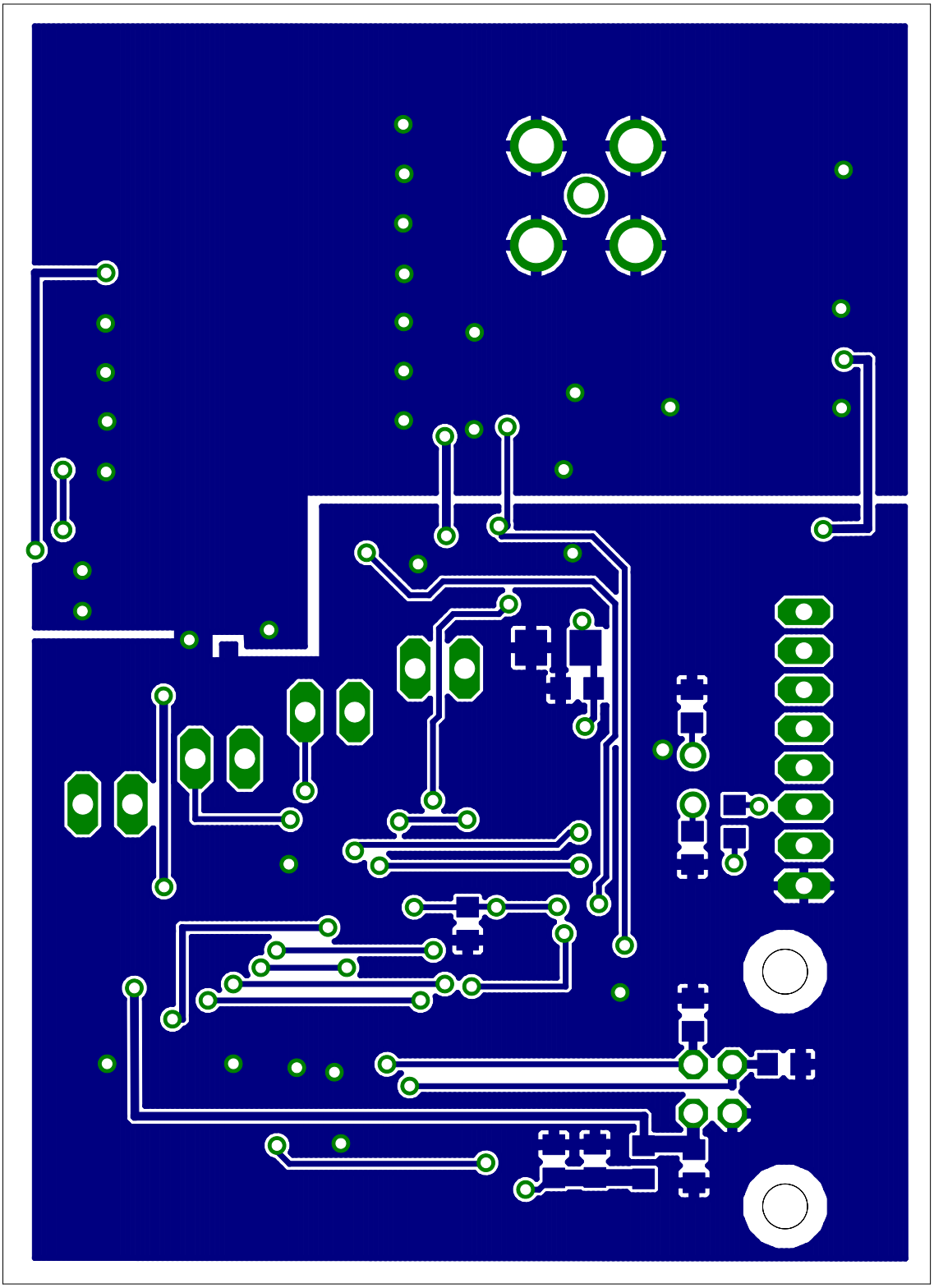

2/14/2008 04:50:32p f=3.14 mirrored C:\Program Files\EAGLE-4.12\projects\SERDP\SERDP RF\RF-B2

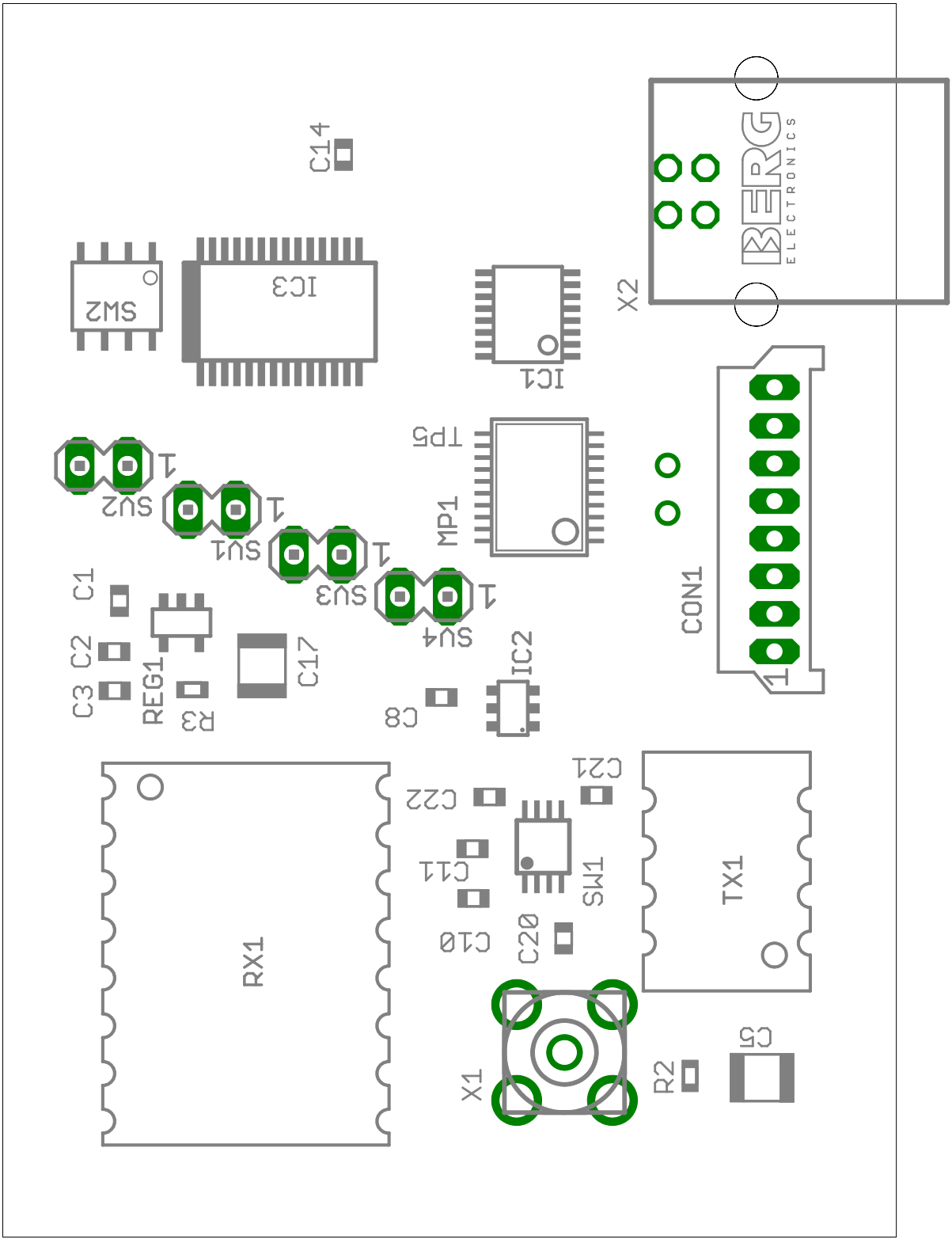
C14
SW2
IC3
IC1
X2
BERG
ELECTRONICS
TP5
MP1
SV2
SV1
SV3
SV4
CON1
C1
C2
C3
REG1
R3
C17
C8
IC2
C21
C22
C11
C10
C20
SW1
TX1
RX1
X1
R2
C5

Partlist exported from C:/Program Files/EAGLE-4.12/projects/SERDP/SERDP RF/RF-B2/SERDP-RF-B2.sch
at 2/14/2008 04:55:01p

Part	Value	Device	Package	Description
C1	0.1 uF	C-USC0603	C0603	CAPACITOR, American symbol
C2	0.01 uF	C-USC0603	C0603	CAPACITOR, American symbol
C3	2.2 uF	C-USC0603	C0603	CAPACITOR, American symbol
C4	10 uF	C-USC1206	C1206	CAPACITOR, American symbol
C5	10 uF	C-USC1210	C1210	CAPACITOR, American symbol
C6	.1uF	C-USC0603	C0603	CAPACITOR, American symbol
C7	47 pF	C-USC0603	C0603	CAPACITOR, American symbol
C8	.1 uF	C-USC0603	C0603	CAPACITOR, American symbol
C9	.1 uF	C-USC0603	C0603	CAPACITOR, American symbol
C10	100pF	C-USC0603	C0603	CAPACITOR, American symbol
C11	100 pF	C-USC0603	C0603	CAPACITOR, American symbol
C12	47 pF	C-USC0603	C0603	CAPACITOR, American symbol
C13	10 nF	C-USC0603	C0603	CAPACITOR, American symbol
C14	0.1uF	C-USC0603	C0603	CAPACITOR, American symbol
C15	0.1uF	C-USC0603	C0603	CAPACITOR, American symbol
C16	4.7uF	C-USC0603	C0603	CAPACITOR, American symbol
C17	10uF	C-USC1210	C1210	CAPACITOR, American symbol
C18	10pF	C-USC0603	C0603	CAPACITOR, American symbol
C19	10 pF	C-USC0603	C0603	CAPACITOR, American symbol
C20	0.1uF	C-USC0603	C0603	CAPACITOR, American symbol
C21	0.1uF	C-USC0603	C0603	CAPACITOR, American symbol
C22	0.1uF	C-USC0603	C0603	CAPACITOR, American symbol
CON1	CON_2MM_8PIN	CON_2MM_8PIN	CON_2MM_8PIN	2 mm Sherlock (tm) connector - 8 pin
IC1	744053BU	744053BU	SSOP16BU	
IC2	SN74LVC1G3157	SN74LVC1G3157	SOT23-6	SPDT switch
IC3	FT245RL	FT245RL	SSOP-28	USB to parallel adapter
L1	Frrite bead	L-USL0603	L0603	INDUCTOR, American symbol
MP1	MSP430F111DB	MSP430F111DB	SSOP20(DB)	MIXED SIGNAL MICROCONTROLLER
Q1		CRYTALTC38H	TC38H	CRYSTAL
R1	47k	R-US_R0603	R0603	RESISTOR, American symbol
R2	10	R-US_R0603	R0603	RESISTOR, American symbol
R3	10	R-US_R0603	R0603	RESISTOR, American symbol
REG1	TPS79333	LDO_REG_SHARP	SOT23-5	Low-dropout regulator - Sharp
RX1	RXM433LR	RXM433LR	RXM433LR	RX module
SV1	MA02-1	MA02-1	MA02-1	PIN HEADER
SV2	MA02-1	MA02-1	MA02-1	PIN HEADER

SV3	MA02-1	MA02-1	MA02-1	PIN HEADER
SV4	MA02-1	MA02-1	MA02-1	PIN HEADER
SW1	PE4230	PE4220	SSOP8	Reflective antenna switch
SW2	MIC2025/75	MIC2025/75	SO-8	Single channel power distribution switch - Micrel
(for	USB)			
TP5	TPSQTP10SQ	TPSQTP10SQ	TP10SQ	
TX1	TXM433LR	TXM433LR	TXM433LR	TX module
X1		BU-SMA-V	BU-SMA-V	FEMALE SMA CONNECTOR
X2		PN61729	PN61729	BERG USB connector

Appendix B

Mechanical design of the system

Pro-E Model for the Floater

Random Angle View

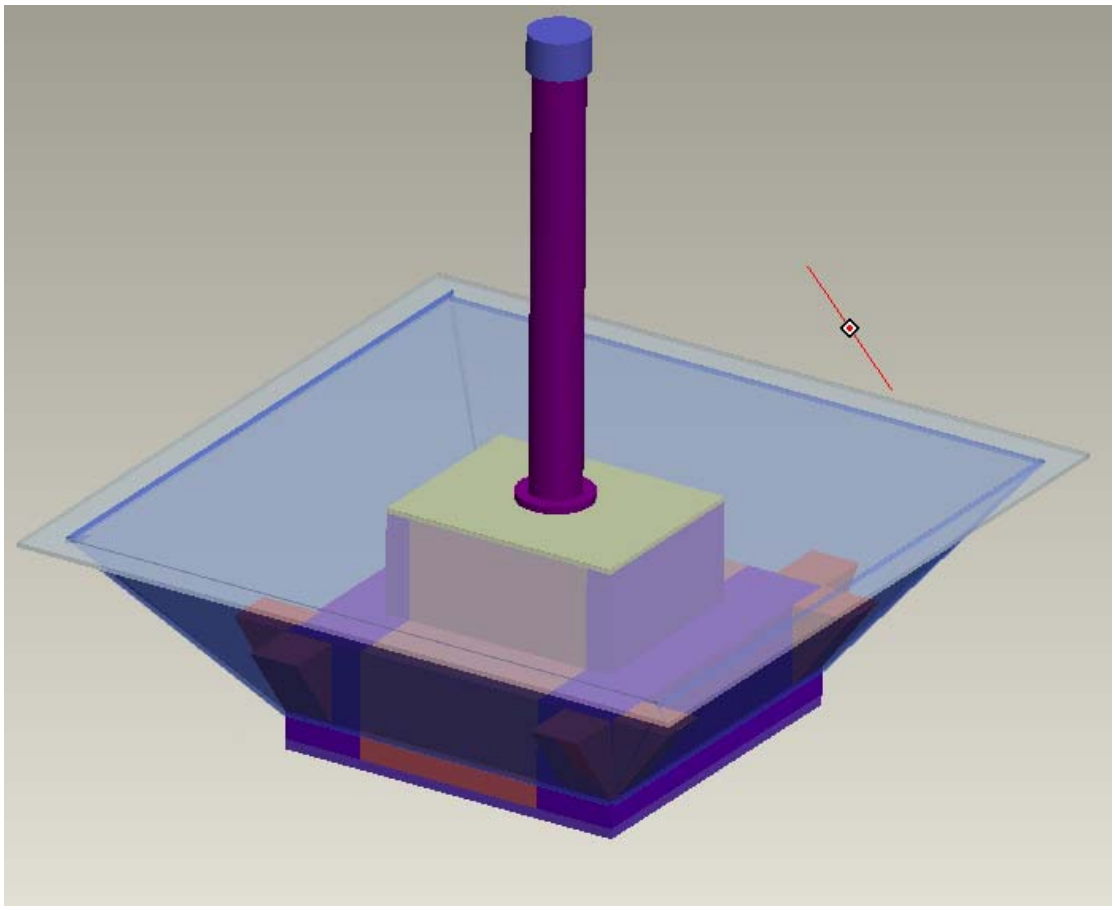

The 2D Assembly Drawing for the Floater

1. Front view

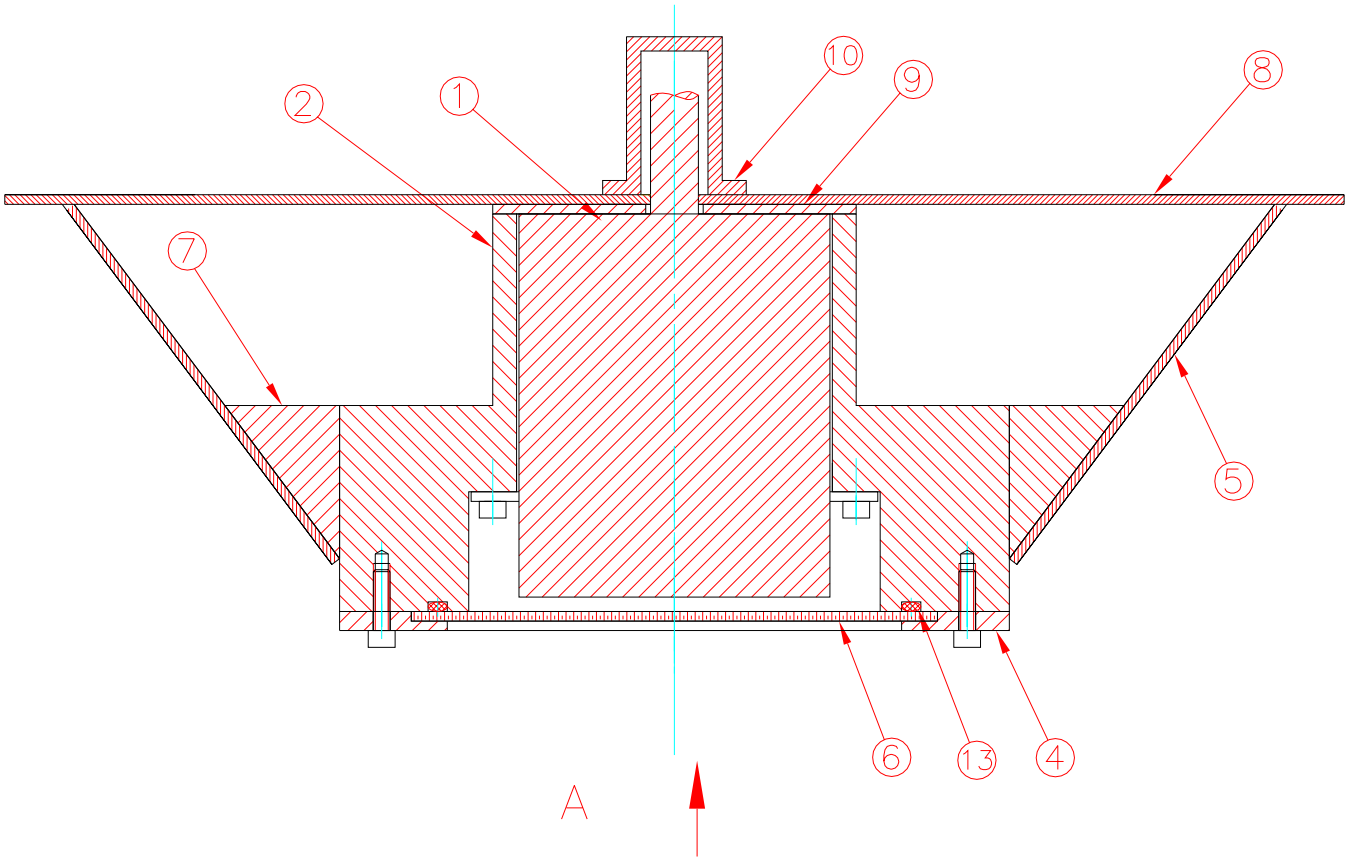

2. Top view

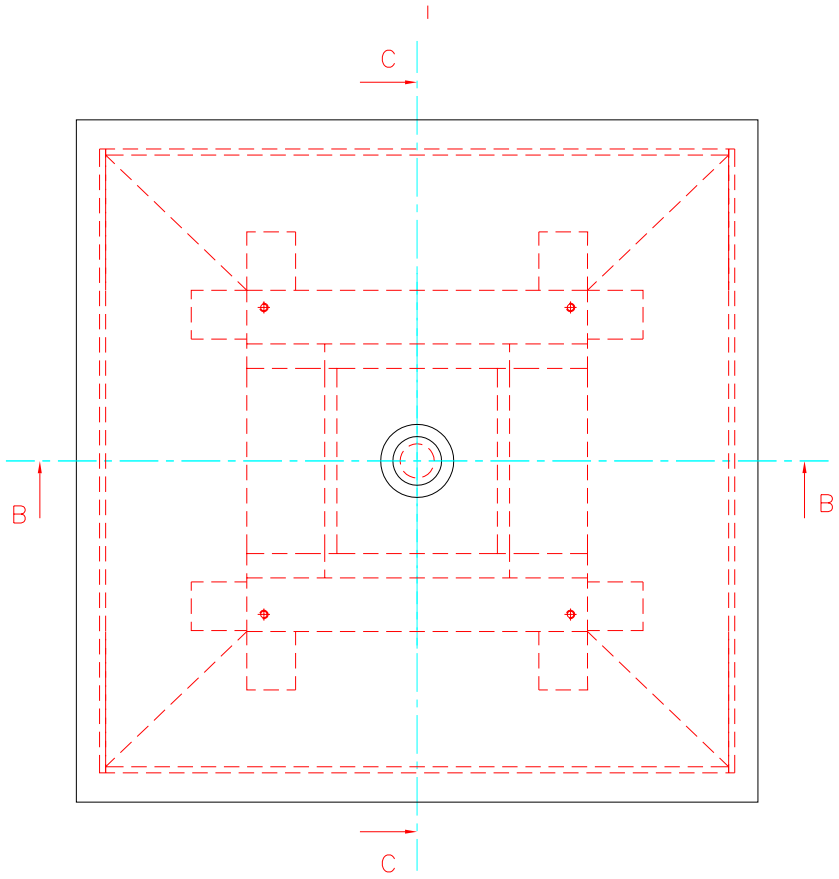

3. Side view

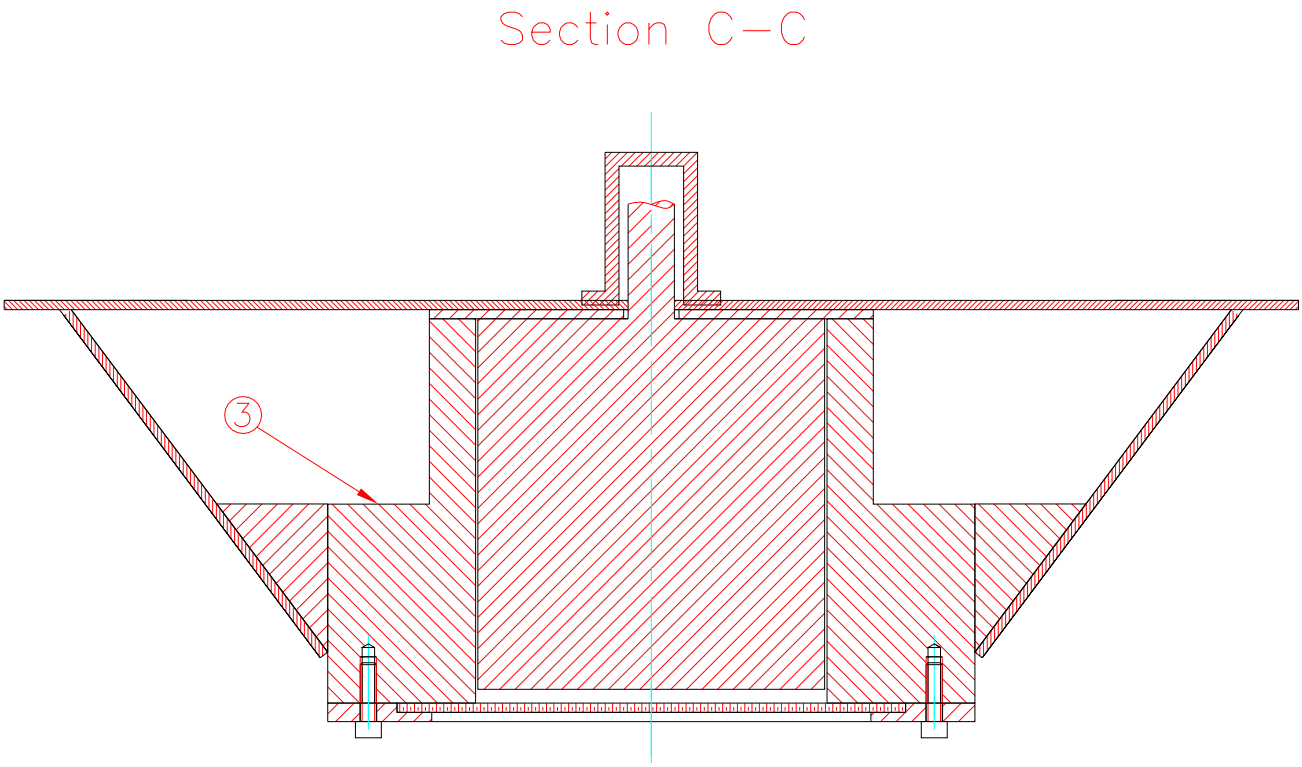

4. Bottom view

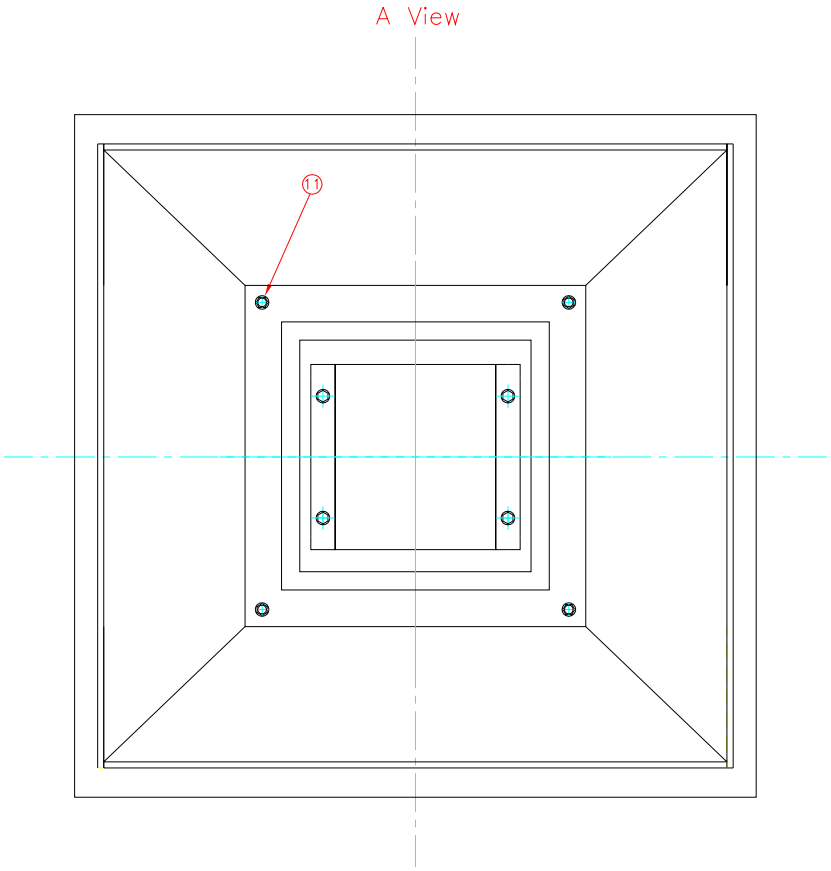

The 2D Drawings for parts of the Floater

1. Cover plate

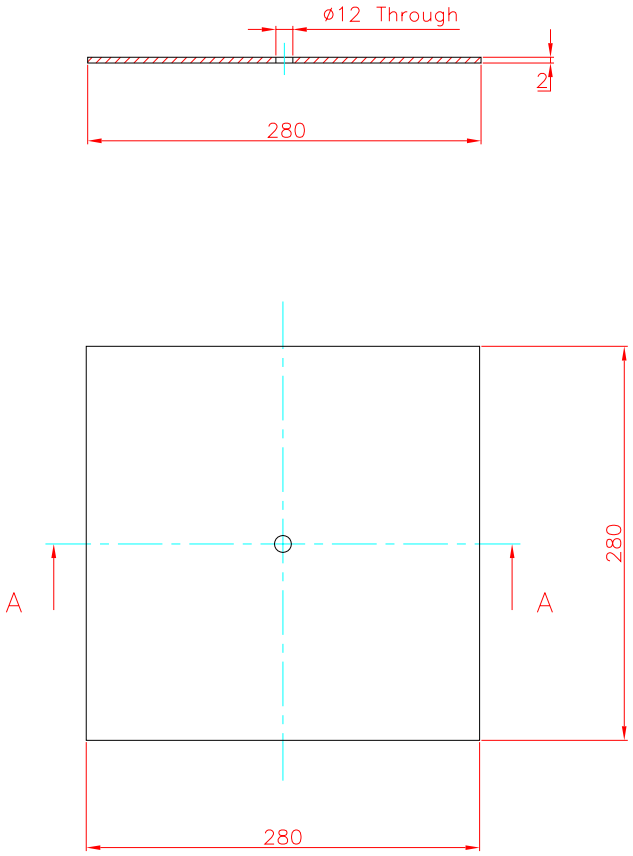

2. Enclosure Part 1

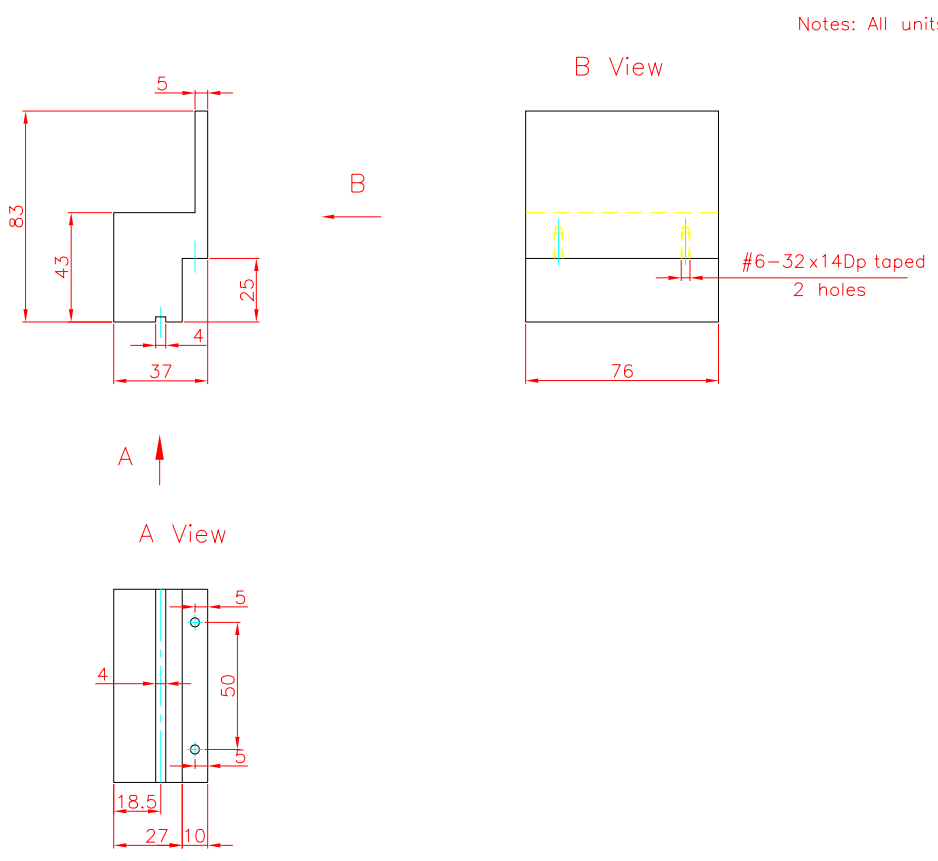

3. Enclosure Part 2

Notes: All units are in Millimeters.

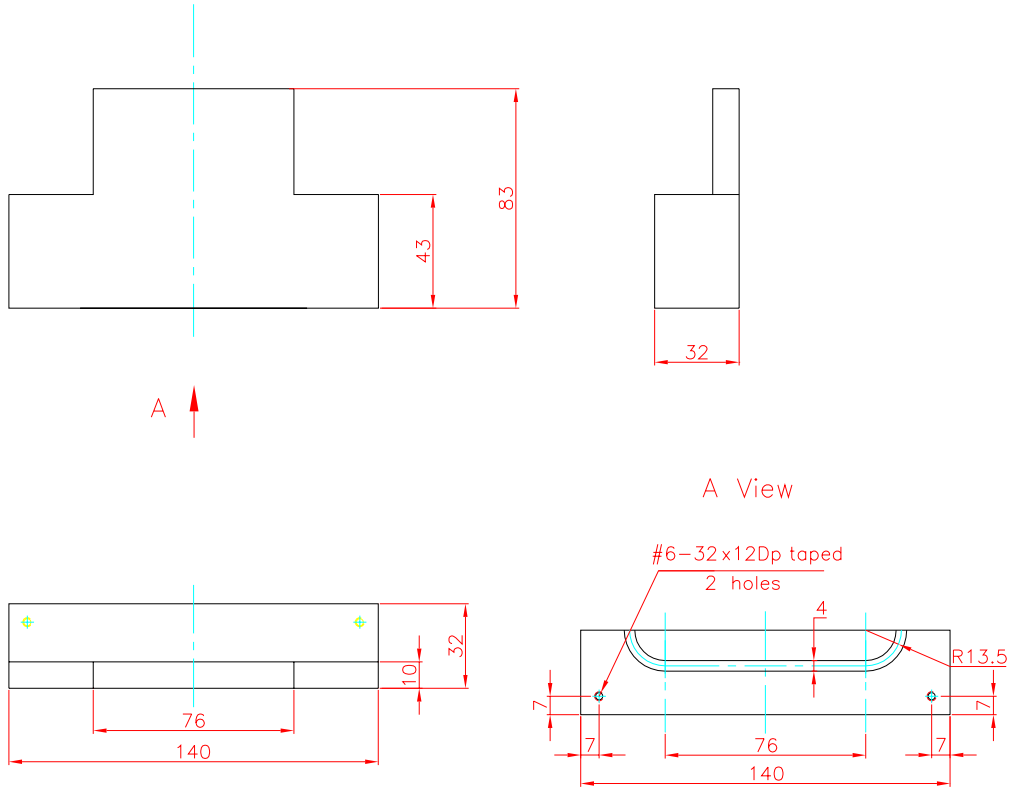

4. Floating Flange

Notes: All units are in Millimeters.

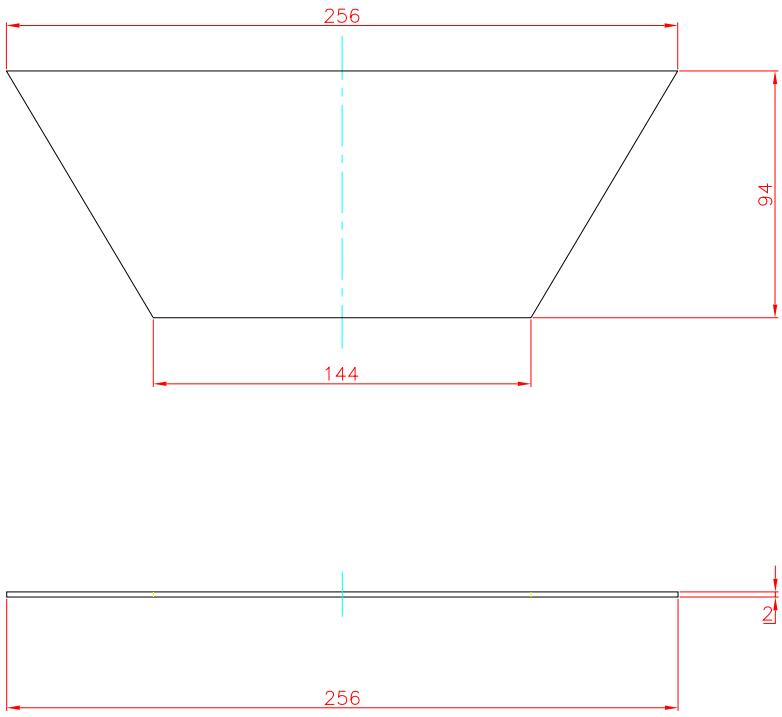

5. Glass Plate

Notes: All units are in Millimeters.

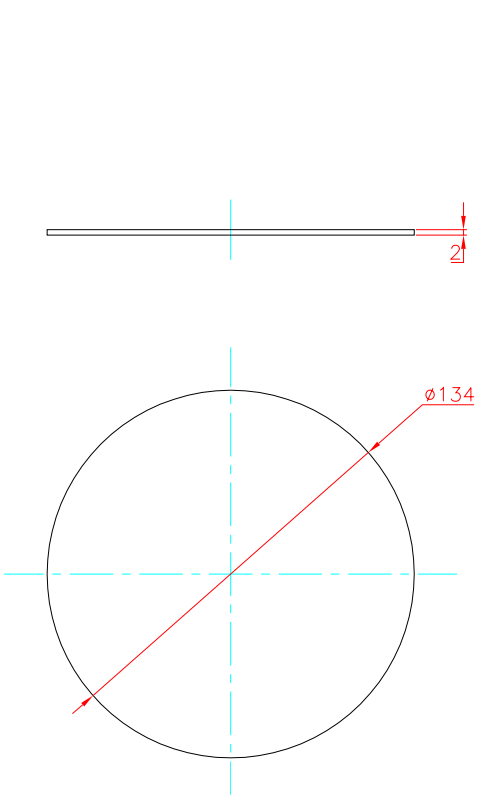

6. Sealing Plate

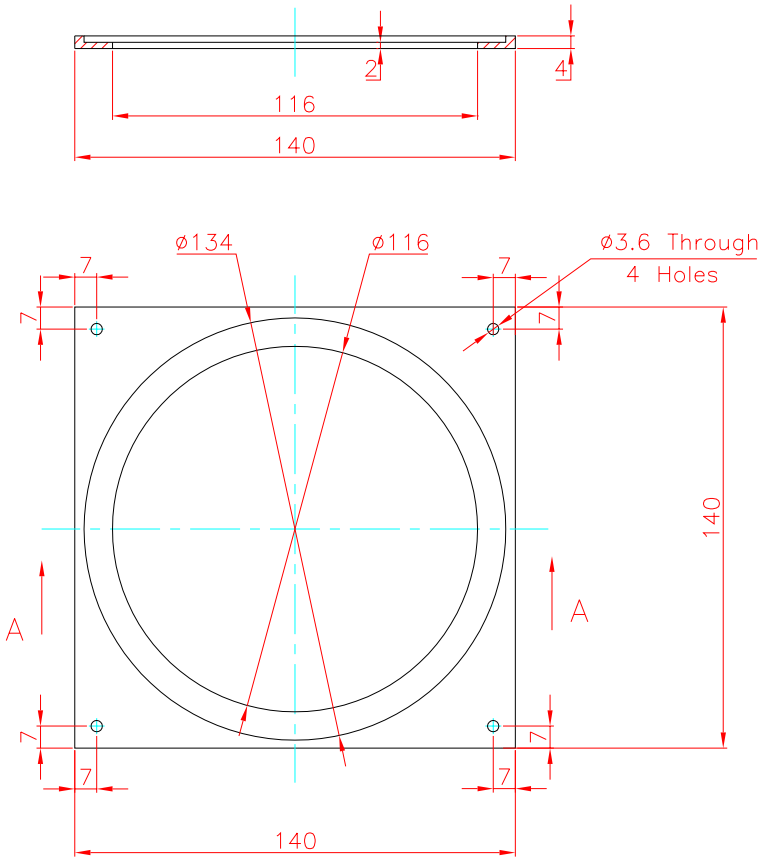

7. Sensor Support Plate

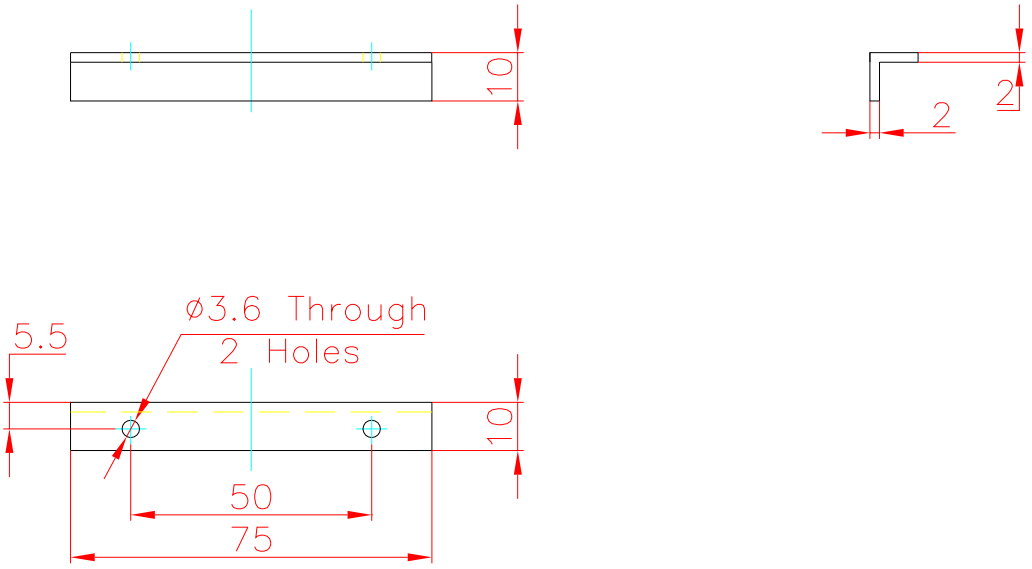

8. Support Plate

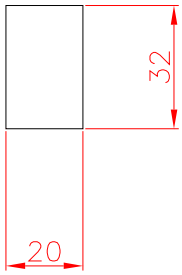

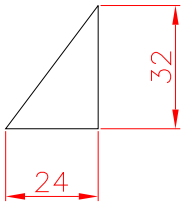

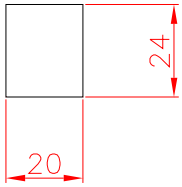

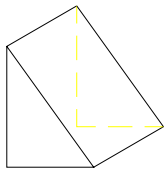

9. Antenna Tube & Cap

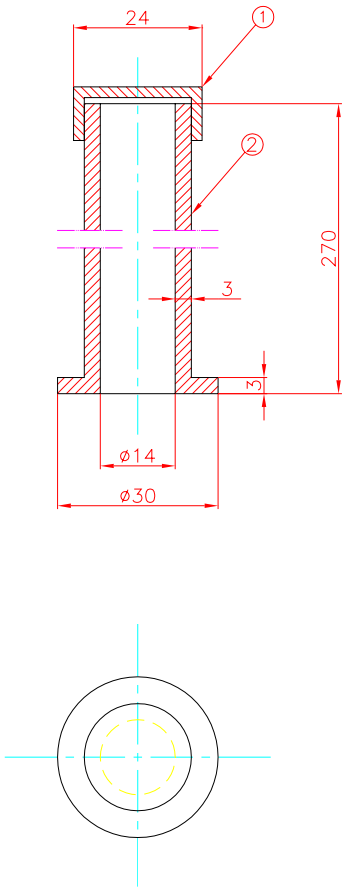

Appendix C

Papers and Presentations

Miniature and low-cost wireless sensor platform for environmental monitoring

Dr. Yordan Kostov and Dr. Govind Rao, Department of Chemical and Biochemical Engineering,
Dr. Upal Ghosh, Department of Civil and Environmental Engineering
University of Maryland Baltimore County, Baltimore, MD 21227

A sensor platform with DO, pH, and turbidity sensors was developed. It was equipped with pH and oxygen sensitive fluorescent foils. The foils were attached outside of the waterproof case and read through optical window. They had also antibiofouling protection, which allowed them to operate for extended period of time. A microcontroller switched the channels and collected the reading of O_2, pH, and turbidity every 15 minutes, than transmitted it through wires interface to a base station. The platform operates from 4 AA size alkaline batteries. The transmitter has a range of approximately 1 kilometer, depending on the terrain, with transmission rate of 10 kbps
The sensor platform is miniature in size (3”x3”x3” sensing head, electronics and battery pack) and low-cost (~ $400/unit).

Presented at **Partners in Environmental Technology Technical Symposium & Workshop, Nov 30-Dec 1, 2006 Washington D.C.**

Miniature and low-cost wireless sensor platform for environmental monitoring

Dr. Yordan Kostov and Dr. Govind Rao, Department of Chemical and Biochemical Engineering,
Dr. Upal Ghosh, Department of Civil and Environmental Engineering

University of Maryland Baltimore County, Baltimore, MD 21227

The main objective of the project is to develop a sensor platform prototype with DO, pH, and turbidity sensors that will have the following capabilities:

The platform has readout optics and electronics equipped with analog to digital converter, microcontroller and transmitter in a waterproof case.

The prototype will provide reading of O_2, pH, and turbidity every 15 minutes and be able to operate from AA size alkaline batteries for extended period of time.

The sensor platform ise miniature in size (3"x3"x3" sensing head and electronics, 4"x4"x1' battery pack) and low-cost (~ $300/unit).

The built-in transmitter will have a range of 1 km, and the transmission rate is 2.4 kbps.

The sensor platform prototype will have adequate anti-biofouling protection, and will be able to withstand continuous field deployment in streams and/or riparian areas.

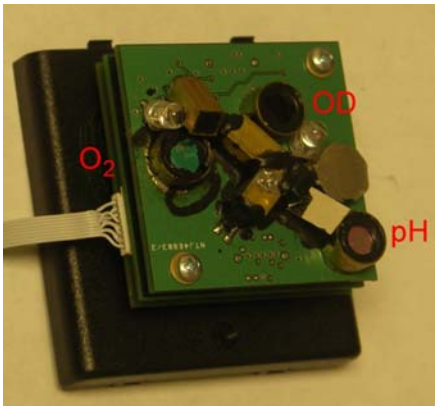

Optical sensor platform. Sensing head with O_2, pH, GFP and turbidity channels.

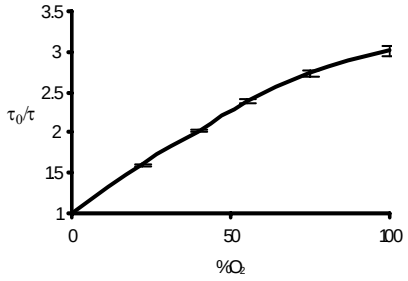

Oxygen sensor calibration curve

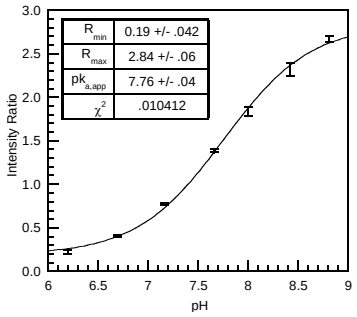

pH sensor calibration curve

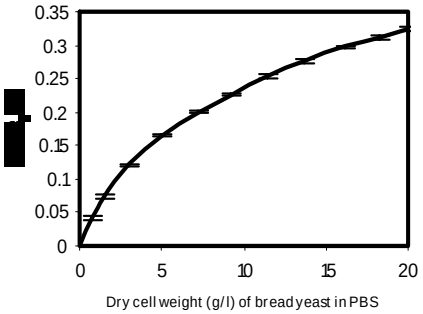

Turbidity sensor calibration curve

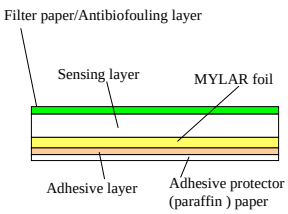

Structure of the sensing foils

Biofouling tests

One month testing of the oxygen sensing membrane for biofouling. At average outdoor temperature of 65 F, no biofouling was visibly detected (with or without antibiofouling layer). More testing is planned at higher temperatures.

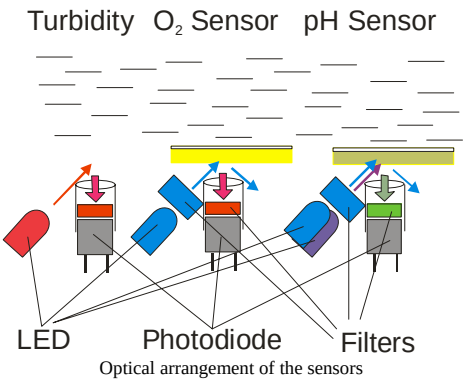

Optical arrangement of the sensors

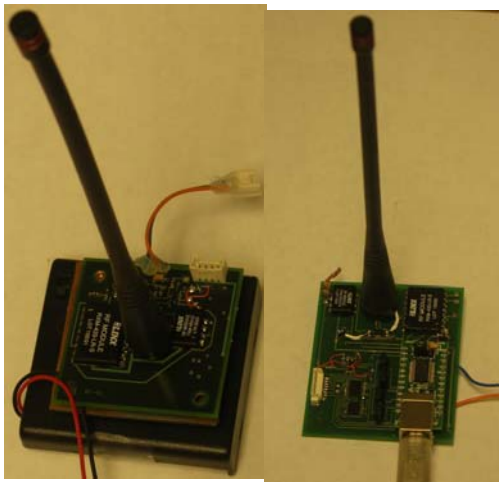

RF communication hardware. A) sensor node; b) base station

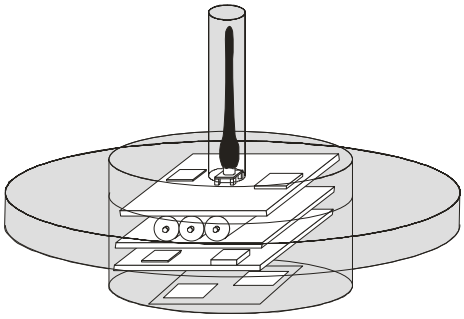

Sensor node floater

Future work

The main components of the platform are developed. Main challenge is sensor calibration at different temperatures. Currently, the components are being integrated into single piece of equipment. Field test are planned.

Wireless sensor network for environmental monitoring based on optical technology

Yordan Kostov, kostov@umbc.edu[1], Upal Ghosh, ughosh@umbc.edu[2], and Govind Rao, grao@umbc.edu[1]. (1) Center for Advanced Sensor Technology, Department of Chemical and Biochemical Engineering, University of Maryland at Baltimore County, 1000 Hilltop Circle, Baltimore, MD 21250, (2) Department of Civil and Environmental Engineering, University of Maryland at Baltimore County, 1000 Hilltop Circle, Baltimore, MD 21250

This work presents the development of a prototype of a sensor for platform environmental networks. The measurement node is designed as a floater. It is equipped with DO, pH and turbidity optical sensors. The pH sensor can be easily replaced by a CO_2 sensor. The sensors are mounted outside on a window. Inside, the platform houses readout optics and electronics equipped with analog-to-digital converter, microcontroller and transmitter in a waterproof case. The prototype provides reading of O_2, pH and turbidity every 15 minutes. It is able to operate from AA size alkaline batteries for an extended period of time. The data are received by a base station, which is operated by a PC (laptop). The base station can address up to 65,000 nodes. The sensor node is miniature in size (3”x3”x3” sensing head and electronics, 4”x4”x1” battery pack), consumes very little power and is low cost. The built-in transmitter has a range of ~1 km and the transmission rate is 2.4 kbps. The sensor platform prototype is able to withstand continuous field deployment in streams and/or riparian areas. The anti-biofouling protection and the longevity of the platform are discussed.

Recent Developments in Sensors and Sensor Networks for Contaminants in Environmental Systems
8:30 AM-11:45 AM, Monday, August 20, 2007 Boston Park Plaza -- Beacon Hill Rm, Oral

Division of Environmental Chemistry

The 234th ACS National Meeting, Boston, MA, August 19-23, 2007

Wireless sensor network for environmental monitoring based on optical technology

Yordan Kostov, Govind Rao, Upal Ghosh

Center for Advanced Sensor Technology
Department of Chemical and Biochemical Engineering
Department of Civil and Environmental Engineering
University of Maryland, Baltimore County

Wireless sensor network

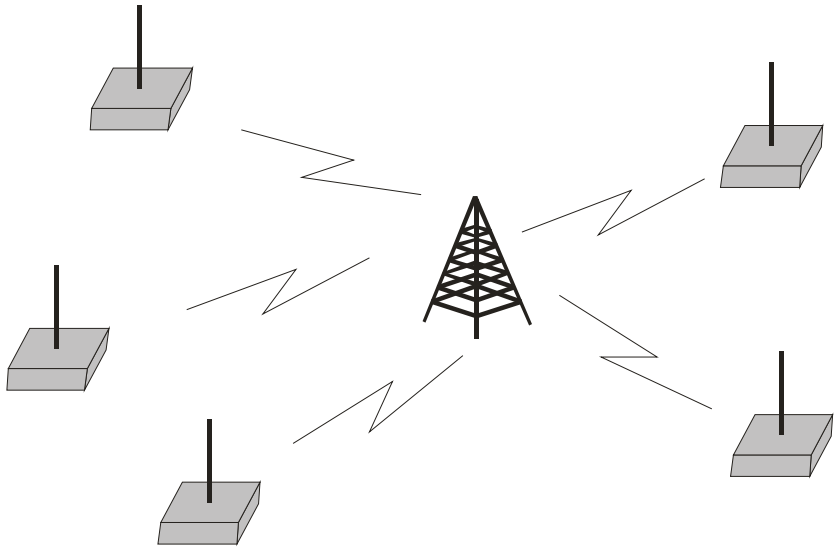

- Sensors are distributed in the observation area
- One base station for all sensors
- Network has star-type structure
- Only one node is queried at a time

Requirements for the network

- Need to observe common environmental parameters
- Wireless = less effort to establish the network
- Many nodes, one base station = simpler infrastructure
- Low maintenance, high reliability and longevity of the nodes needed
- Reliable sensors!
- Low-cost?

Measurements of DO, turbidity and pH

- Oxygen concentration is typically measured using Clark electrode (amperometric measurement) or using Winkler's method (chemical assay)
- Turbidity is measured optically (measurement of back reflected or/and scattered light)
- pH (acidity/basicity) is measured using pH electrode (potentiometric measurement) or using indicator strips (another chemical assay)
- The measurements are based on several different methods and their integration on a single platform is technologically challenging (3 different devices needed)
- However, this is necessary if an environmental network is to be deployed!

Optical sensor technology

- The 3 measurements (DO, pH, OD) can be performed optically using optical sensor technology
- Some optical sensors for DO and pH are already commercially available

- ➢ Optical sensors are robust
- ➢ Optical sensors work in equilibrium (no analyte or material consumed)
- ➢ Optical sensors are easily miniaturized and can fit on any current platform
- ➢ They can be read using the same device (photometer) which reduces the device count
- ➢ No direct electrical contact with the sensors

Optical oxygen sensor principle

Oxygen dynamically quenches luminescence with decay rate >20 ns
Fluorescence lifetime *t* is decreased:

$$\frac{\tau_0}{\tau} = 1 + k_{SV}[O_2]$$

$$\tan\ \varphi = \omega \cdot \tau$$

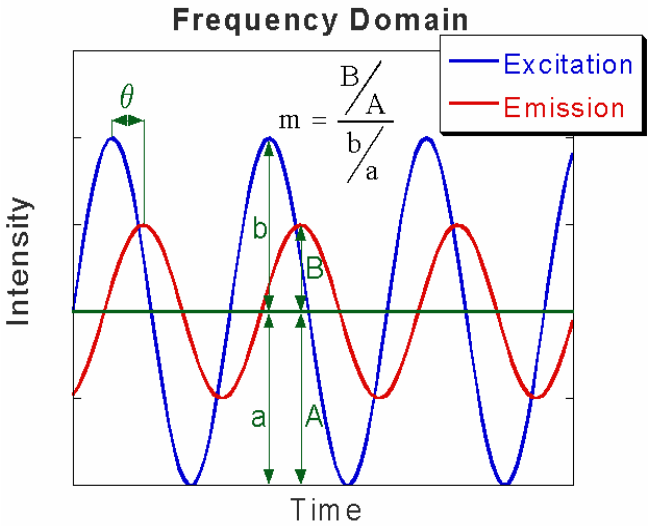

If the excitation light source is sinusoidally modulated in intensity, intensity of the emission follows the same pattern. Fluorescence lifetime creates a time lag, which appears as a phase shift and decreased modulation.

Tolosa, L., Kostov, Y., Harms, P., Rao, G. (2002) *Biotech. Bioeng.***80**, 594-597.

Oxygen sensor

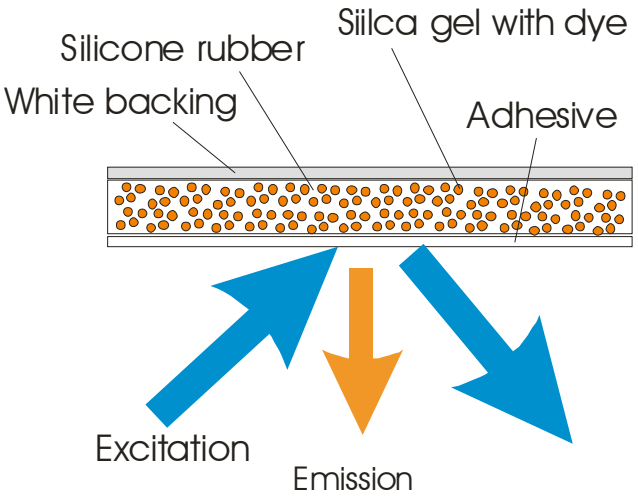

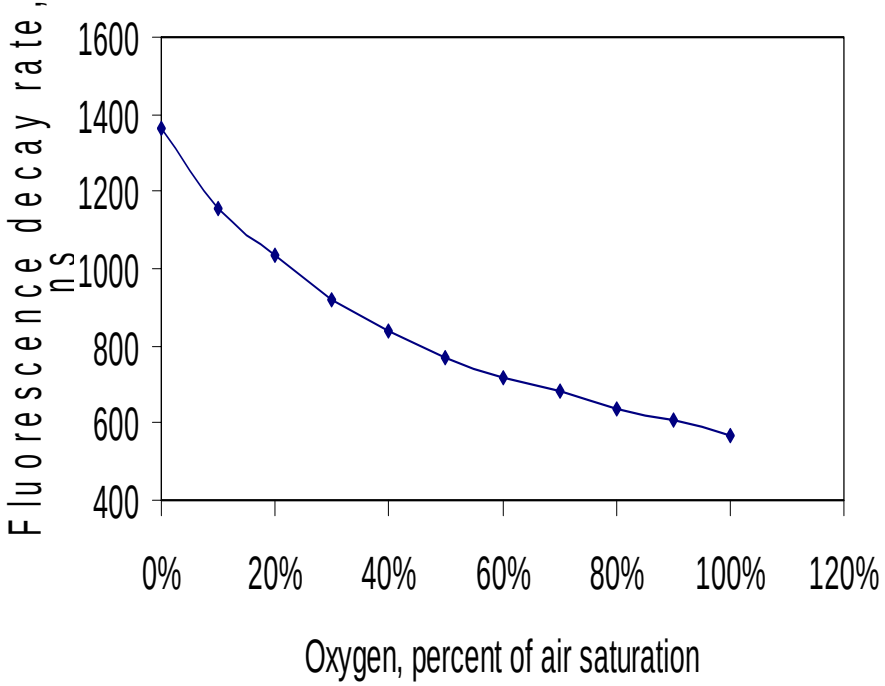

- Ruthenium dye, lifetime: 1.39 μs in absence of oxygen
- Excitation – 470 nm, emission – 630 nm
- Immobilized on silica gel and embedded in silicone rubber
- White optical shield prevents unwanted interferences

Oxygen sensor - calibration

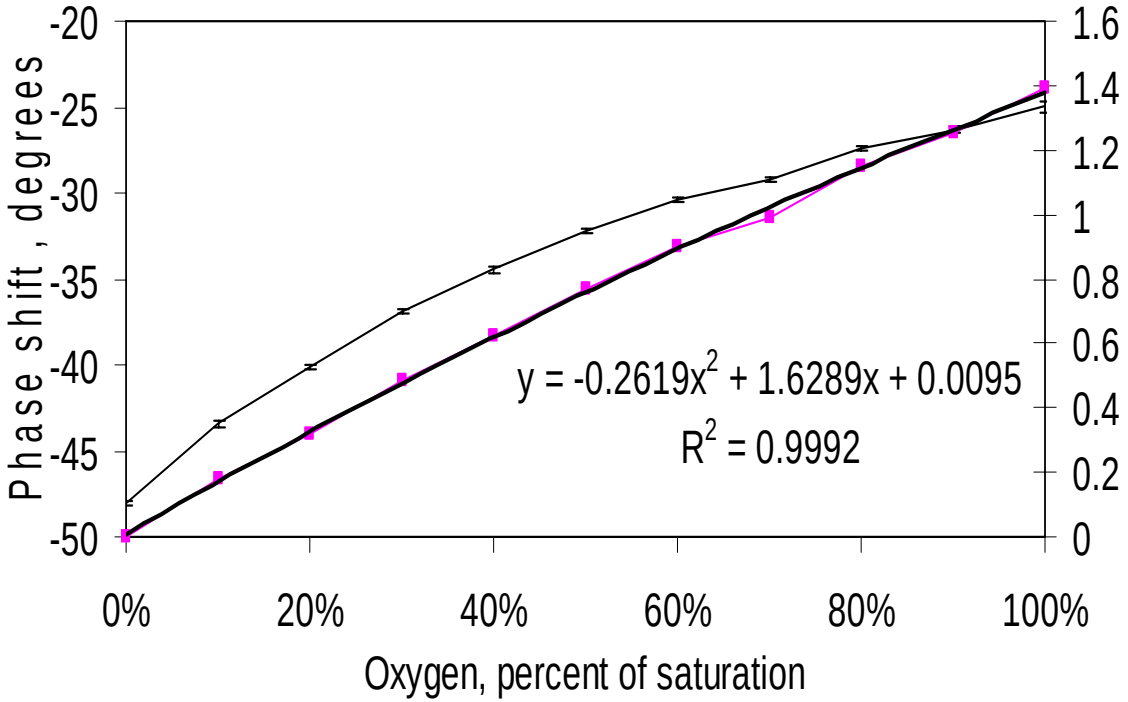

- The whole batch of patches is calibrated
- Phase shift: ~2^{O}/10% O_2,
- Accuracy of the measurement – <1% O2
- SD of phase measurement - 0.15 degrees

Optical pH sensor principle

pH indicator is a weak acid which dissociation is function of the environmental pH

$$[HA] \leftrightarrow [H+] + [A-]$$

$$pH \sim \frac{[HA]}{[A^-]}$$

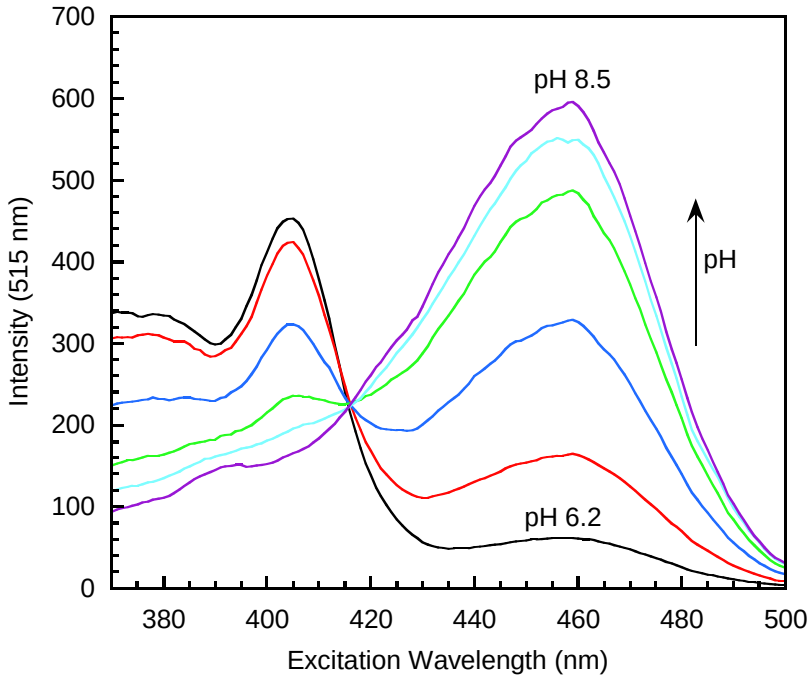

With fluorescent pH indicator like HPTS, change in environmental pH results in different excitation spectra. The pH is related to the emission ratio when the sensor is excited at the respective excitation maxima.

Kermis, H.R., Kostov, Y., Rao, G. (2003) *Analyst* **128**, 1181-1186

Kermis, H.R., Kostov, Y., Harms, P., Rao, G. (2002) *Biotechnol. Prog.* **18**, 1047-1053

pH sensor

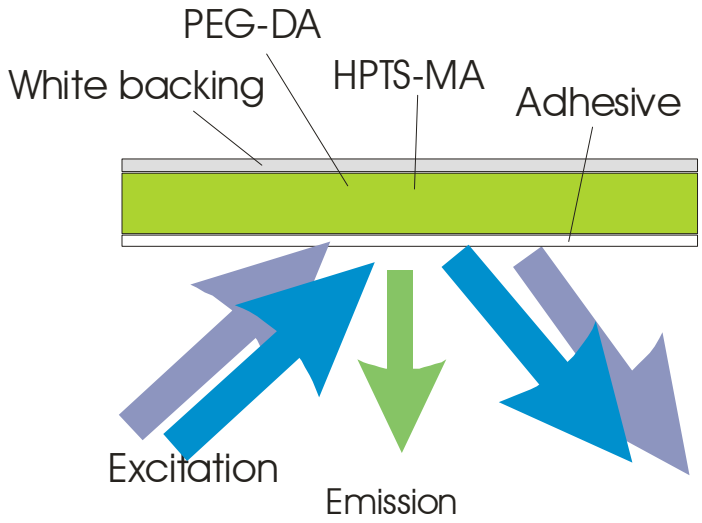

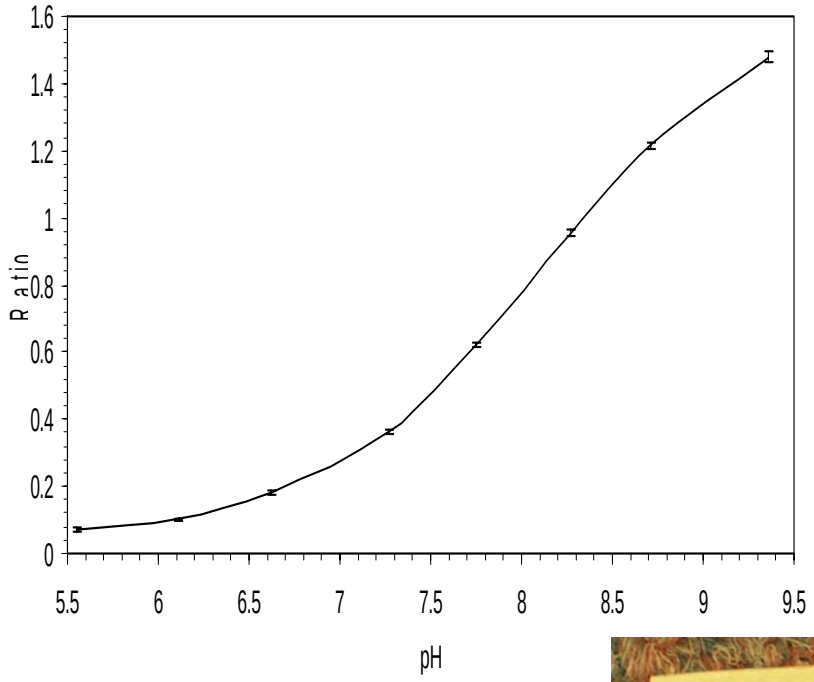

- Dye – HPDS-MA (pH indicator derivatized with methacrylate group)
- Dye excited at 405 and 455 nm, emission ratio at 535 nm monitored
- Dye immobilized in PEG hydrogel, gel placed on special carrier.
- White optical shield is permeable for water and ions
- Whole batch of patches is calibrated.

Turbidity sensor

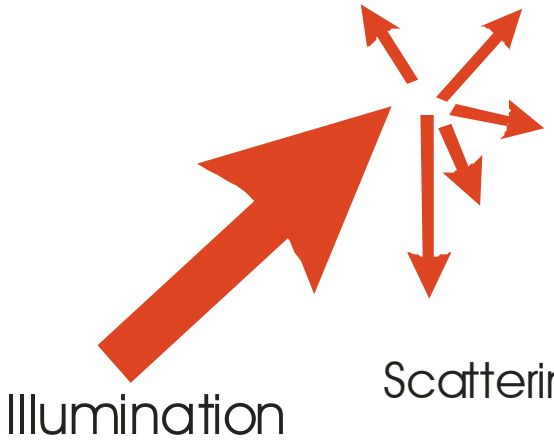

$$\text{Turbidity} \sim \lg \frac{I}{S}$$

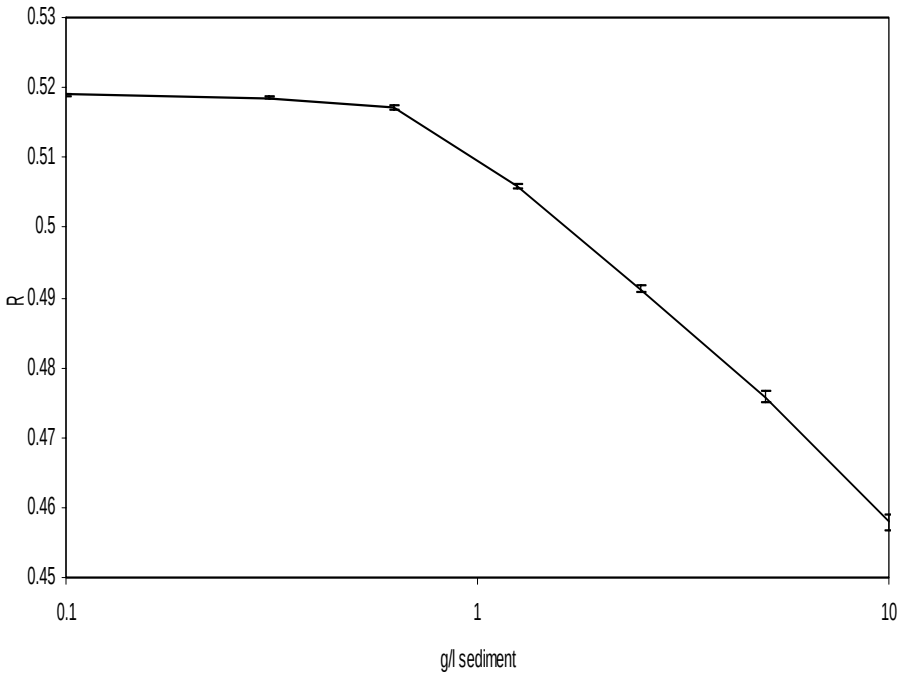

- Turbidity is measured as degree of backscattering of the illumination light
- It is usually referenced to the intensity of the illumination light
- Turbidity strongly depends on the optical path and usually requires individual calibration.

Optoelectronics

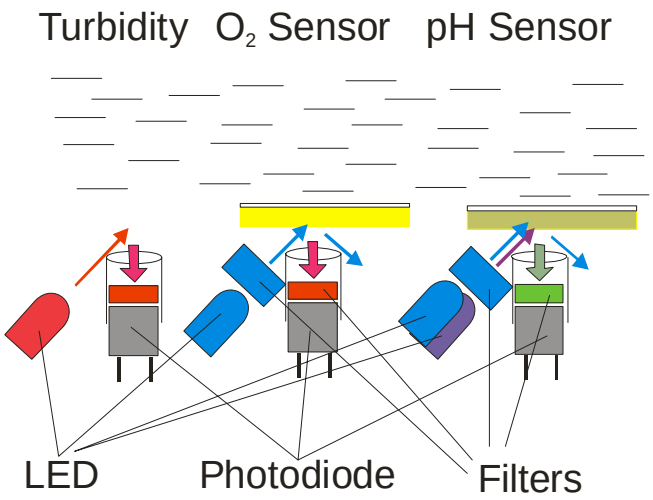

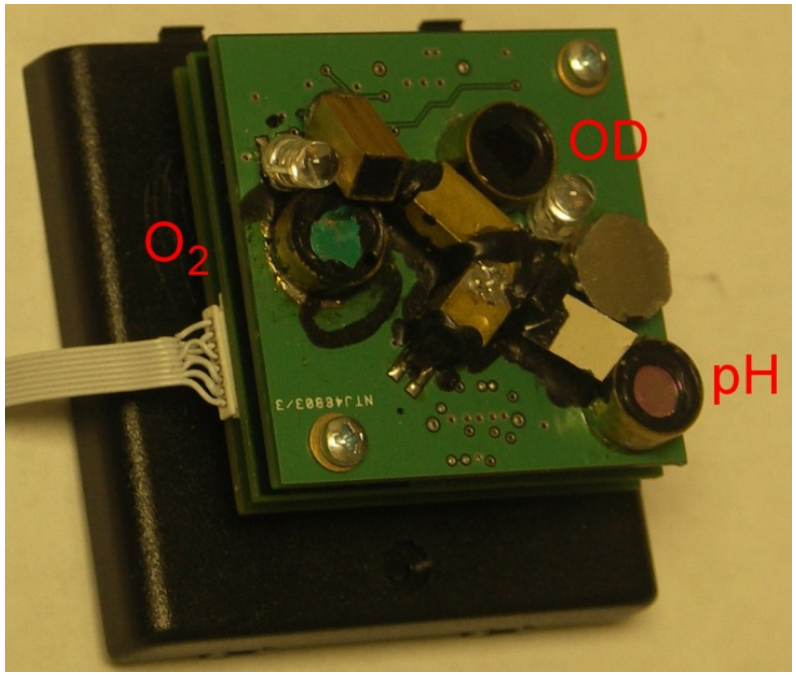

- The sensors are excited using LEDs
- The fluorescence or scattered light is detected using semiconductor photodiodes
- Both the excitation and emission light is filtered using bandpass interference filters
- The LEDs are fired sequentially in order to prevent the crosstalk between the sensors
- The optical paths for the sensors are positioned specifically to avoid crosstalk

Sensor node - structure

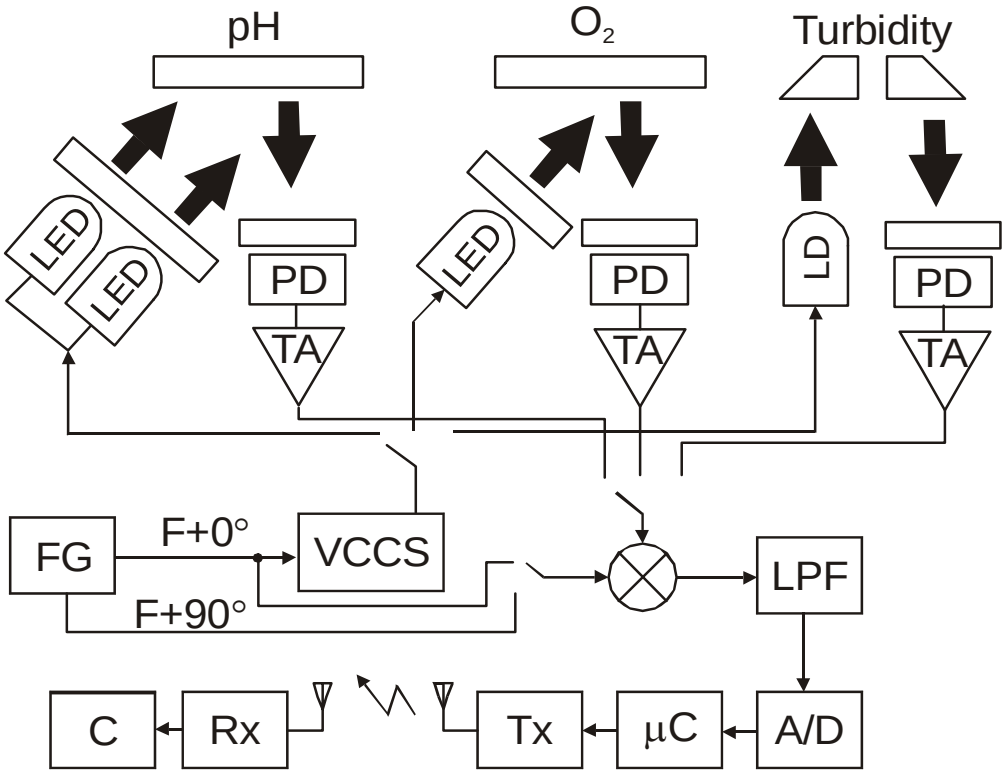

PD – photodiode, FG – Frequency generator, ⊗ - multiplier, µC – microcontroller, Tx – transmitter, Rx – receiver, C – computer.

- The LEDs are modulated to allow the extraction of the signal
- The amplitudes or the phase angles are determined using Lock-in amplifier
- The signal is digitized using 16-bit ADC
- A microcontroller acquires the signals and sends them over wireless connection
- The data are received at base station and transferred to a computer for data manipulation and display

Sensor Node – Control and RF

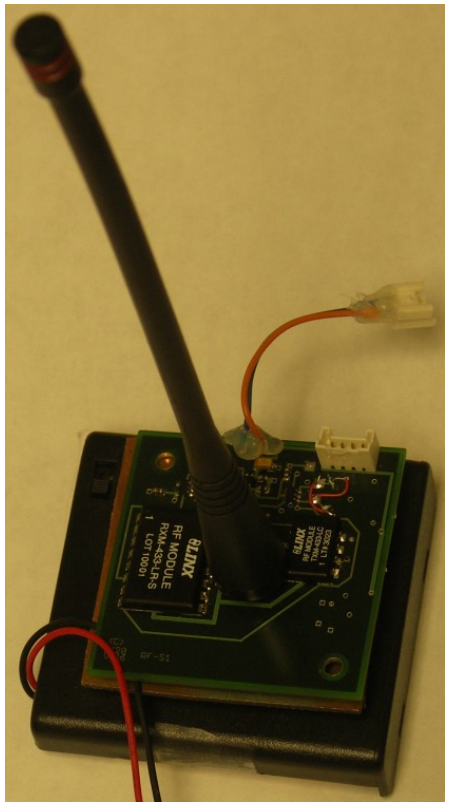

- Dedicated ultralow power (MSP430F2013) microcontroller is used
- Control programs are written in Assembly
- RF transceivers operate at 430 MHz (penetrates concrete)
- The measuring cycle is initiated only at request from the base station
- If the node number is recognized, the controller turns of RF and cycles through the sensors
- The data are sent back to the base station

Sensor Node – Power Budget

- The sensor node is powered from 4 AA batteries
- The power use during 1 measurement cycle is 0.033 mAh
- The power use during 1 transmit/receive cycle is 0.0006 mAh
- At battery capacitance 1700 mAh, this would suffice for ~ 50 000 measurements
- At rate 5 measurements/h, the battery should last a little over an year
- We have observed the battery to last ~ 2 months with the receiver constantly on

RF wireless protocol

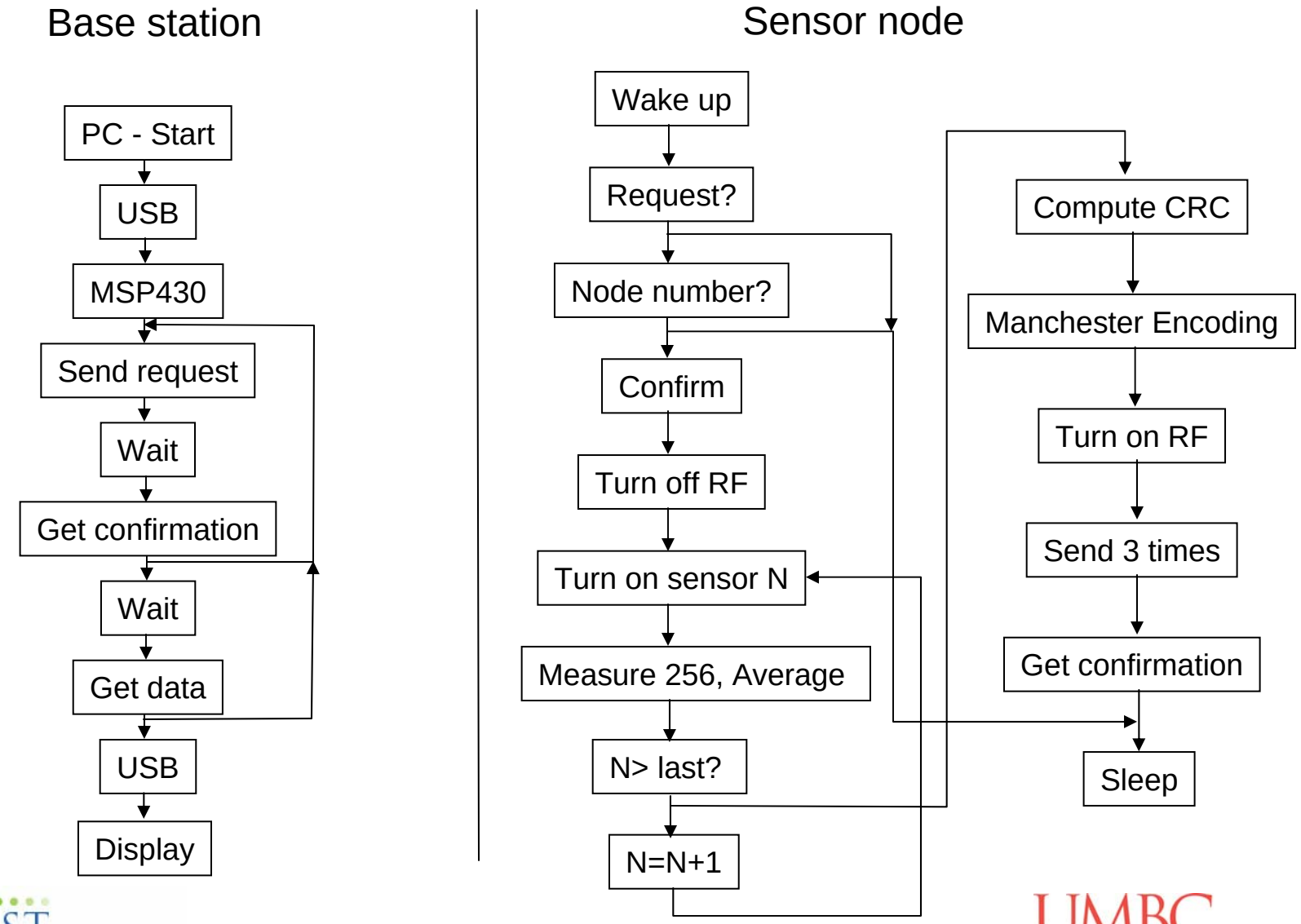

Sensor node - floater

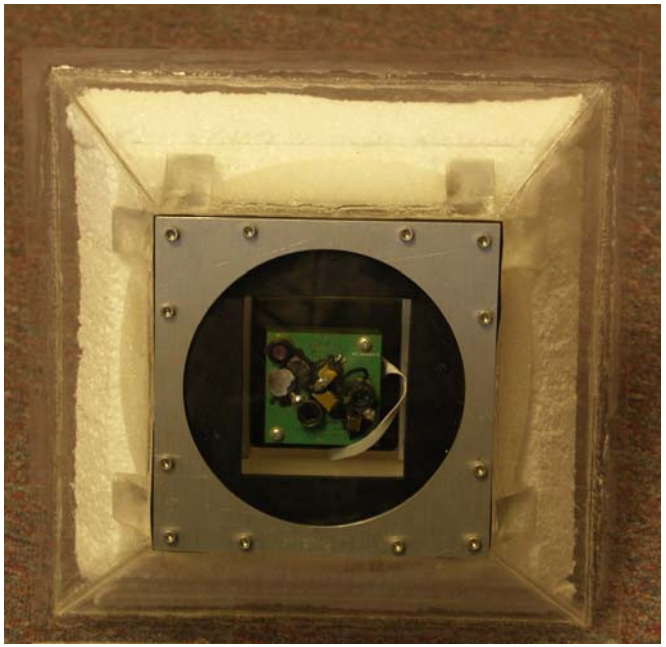

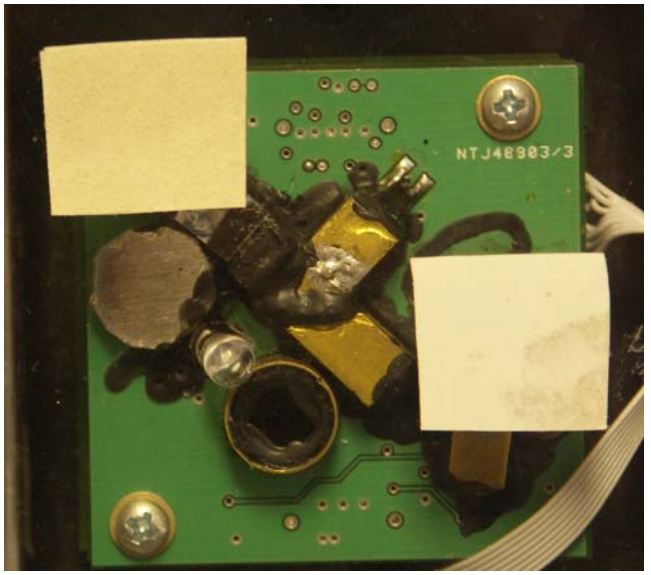

- The electronics is enclosed in water-proof case
- The case is designed to float half submerged
- The bottom window caries the installed sensor patches
- The antenna stays out of the water to ensure effective transmission to the base station

Sensor node – measurements

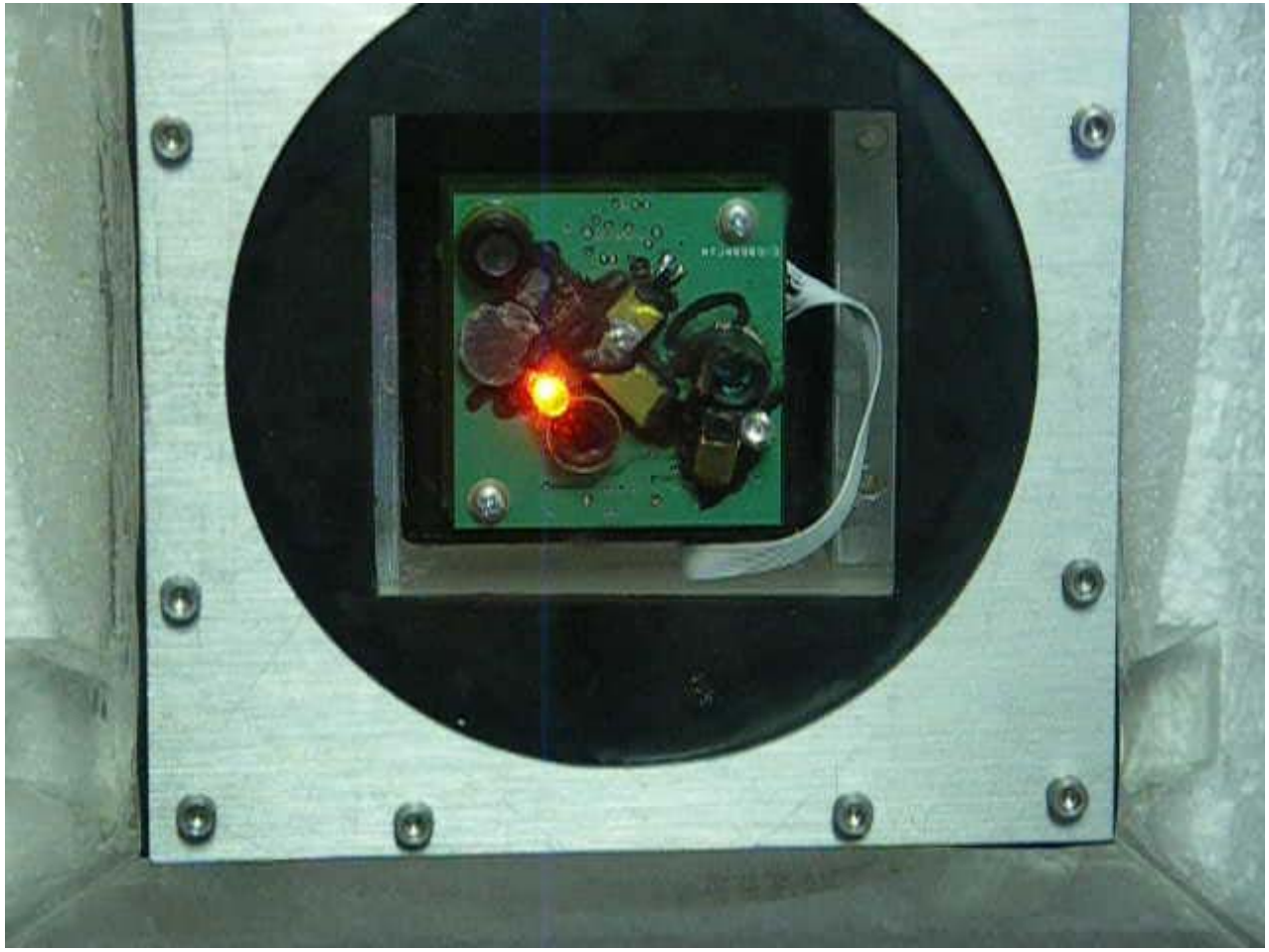

Base station

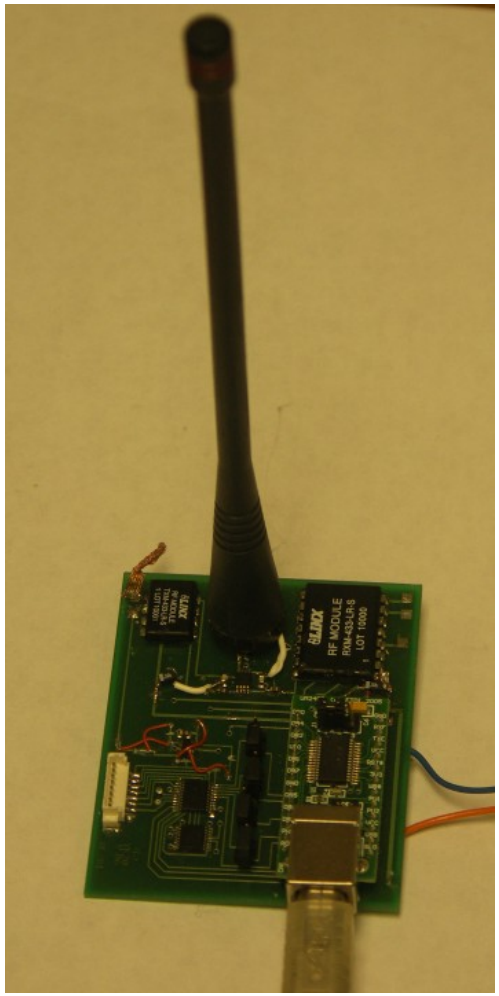

- Base station provides a bridge between the sensor and the host computer
- Microcontroller (MSP430F1121A) communicates with the PC through USB adapter
- At request, it sends the measurement request to the specific node via RF
- Data transmission is Manchester encoded
- Data rate : 2.4 kBaud
- Error detection: CRC
- Error correction: repeat 3 times, if incorrect, request the data again
- Frequency: 433 MHz (ISM band)
- Distance: open country ~ 600 yards, indoor ~ 200 yards

PC interface

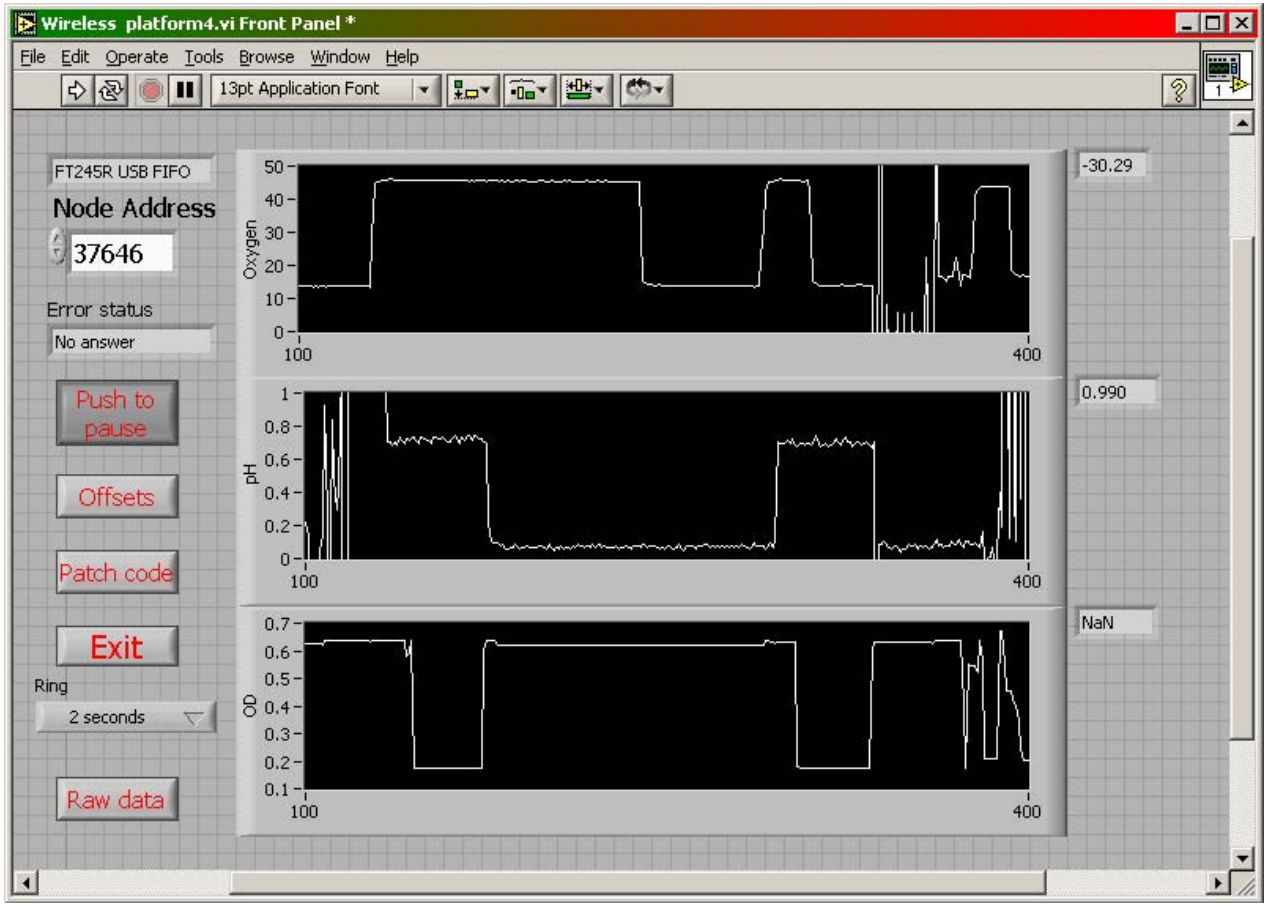

- Labview based
- Allows to select the node by number
- Offsets, calibration
- Time interval between the data acquisition
- Graphical and numerical output

Tests

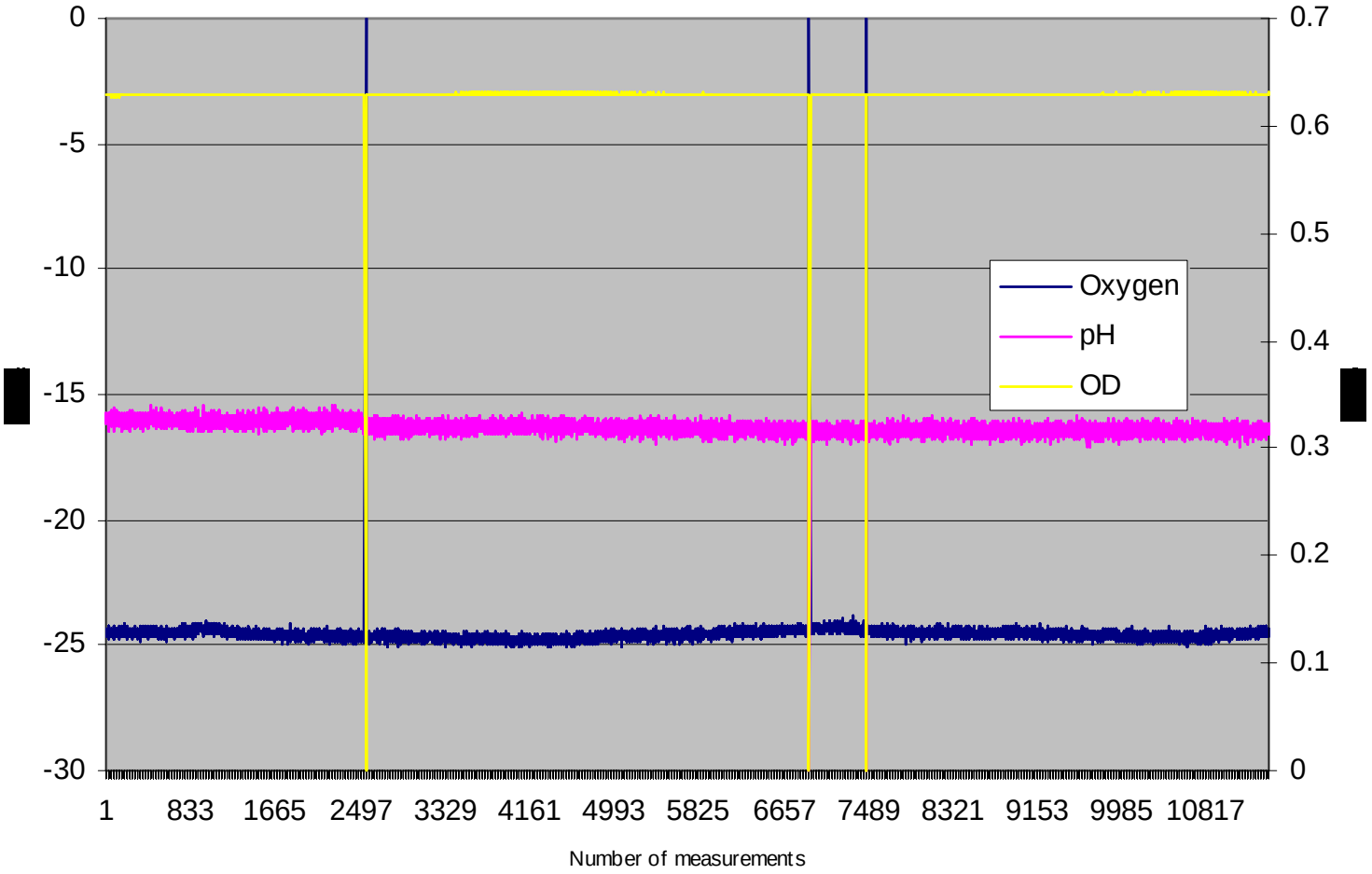

- Presented data show the equivalent of 3 months of continuous measurements (once every 15 minutes)
- The pH sensor: <0.02pH drift, NOT sensitive to temperature (< 0.02% change/^{o}C)
- Oxygen sensor: <3%O_2 drift, 2.6%/^{o}C (easily correctable through calibration)

Future work

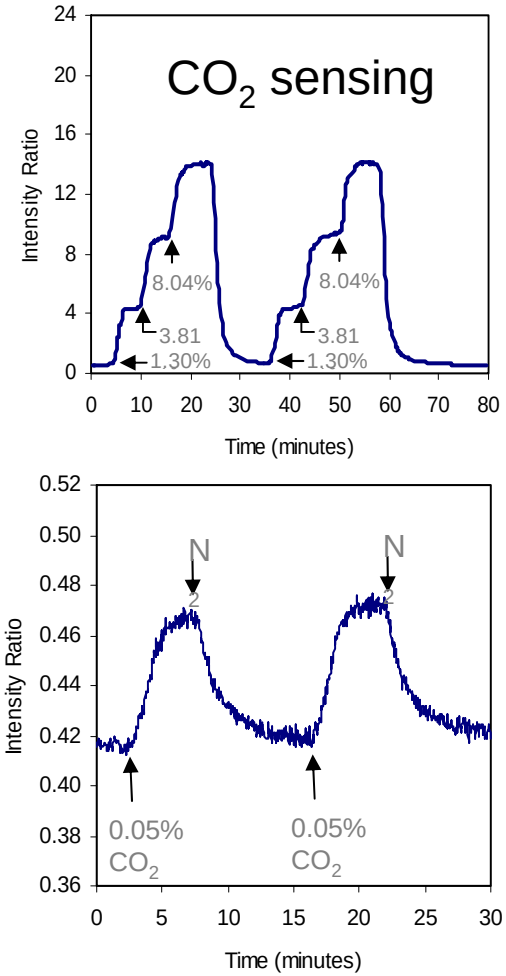

- Sensor-to-sensor communication
- Better energy-conserving algorithms
- Energy harvesting hardware (solar cell, turbine?)
- New sensors (CO_2 available)
- Continuous deployment of many sensors
- Tests, tests, tests!

Conclusion

- **Highly reliable** sensor platform for DO, pH, and turbidity measurements for monitoring streams and/or riparian areas is developed
- The prototype provide reading of **O_2, pH, and turbidity** every 15 minutes and is able to operate from AA size alkaline batteries for extended period of time.
- The sensor platform is **small and low-cost**.
- The built-in transmitter has a range of 600 yards, and the transmission rate is 2.4 kbps.

Credits

- Dr. Appa Anjanappa
- Dr. Ramachandram Badugu
- Raghavendra Angara
- Jingrui Wang
- Albert Hsu
- Sherif Ibrahim

- Strategic Environmental Research and Development Program (SERDP)
- DoD
- DoE
- EPA

- NIH, NSF, industry